



รายงานวิจัยฉบับสมบูรณ์

โครงการโครงสร้างระดับจุลภาคและคุณสมบัติของคาร์บอนคล้ายเพชร

โดย อ. ดร.สิริโชค จึงถาวรรณ และคณะ

รายงานวิจัยฉบับสมบูรณ์

โครงการโครงสร้างระดับจุลภาคและคุณสมบัติของคาร์บอนคล้ายเพชร Microscopic structures and properties of diamond-like carbon

คณะผู้วิจัยและสังกัด

อ. ดร.สิริโชค จึงถาวรรณ

ศ. ดร.ชูกิจ ลิมปิจำนงค์
สาขาวิชาฟิสิกส์ มหาวิทยาลัยเทคโนโลยีสุรนารี

สนับสนุนโดยสำนักงานคณะกรรมการการอุดมศึกษา และสำนักงานกองทุนสนับสนุนการวิจัย (ความเห็นในรายงานนี้เป็นของผู้วิจัย สกอ. และ สกว. ไม่จำเป็นต้องเห็นด้วยเสมอไป)

บทคัดย่อ

คาร์บอนอสัณฐาน (amorphous carbon) เป็นรูปโครงสร้างหนึ่งที่มีการเรียงตัวของอะตอมแบบโครงข่ายที่ไม่มีระเบียบ โครงสร้าง หนึ่งที่เสถียรคือคาร์บอนคล้ายเพชร (diamond-like carbon, DLC) ประกอบด้วยพันธะเคมีแบบ sp³ เป็นส่วนมากทำให้มีคุณสมบัติส่วนมาก คล้ายกับเพชร เช่น มีค่าแถบพลังงานกว้าง (wide bandgap) มีความแข็งสูง และเฉื่อยต่อปฏิกิริยาเคมี อย่างไรก็ดีเนื่องจากโครงสร้างของ คาร์บอนอสัณฐานไม่เป็นระเบียบและระบบที่มีการเรียงตัวขนาดเล็กมีความซับซ้อน การศึกษาโครงสร้างระดับอะตอมของระบบที่ไร้ระเบียบ จึงมีน้อย ความรู้ความเข้าใจในโครงสร้างของระบบดังกล่าวจึงจำเป็นอย่างยิ่งต่อการศึกษาสมบัติต่าง ๆ ของวัสดุ แบบจำลองโครงสร้างของ ระบบที่ไร้ระเบียบจึงเป็นสิ่งสำคัญในการทำนายคุณสมบัติของวัสดุ แบบจำลองทางทฤษฎีช่วยให้สามารถวิเคราะห์คุณสมบัติของสารโดยมี ความชัดเจนมากขึ้นกว่าการประมาณที่ใช้กันอยู่ในปัจจุบัน เมื่อได้แบบจำลองโครงสร้างแล้ว การคำนวณคุณสมบัติอื่น ๆ ก็สามารถทำได้ เช่น สามารถเพิ่มสารเจือของธาตุอื่นเข้าไป ทำให้ทราบแนวทางในการปรับเปลี่ยนคุณสมบัติของสารและพื้นผิวหรือแม้แต่ทราบได้ว่าสาร แปลกปลอมชนิดใดที่ต้องให้ความระวังสูงเพื่อเป็นข้อมูลในการประยุกต์ศึกษาวิจัยในแง่มุมอื่นต่อไป

โครงการนี้ได้ศึกษาแบบจำลองโครงสร้างที่ส่งผลสำคัญต่อวัสดุ โดยการวิเคราะห์โครงสร้างของสารต่าง ๆ ที่เกี่ยวข้องกับคาร์บอน โดยใช้ระเบียบวิธีการคำนวณแบบเพิร์สพรินซิเพิล ในช่วงเริ่มโครงการได้ทำการศึกษาผลของการเรียงตัวในระยะสั้น ๆ ระดับจุลภาคเนื่องจาก พันธะอะตอมที่แตกต่างและการเรียงตัวของอะตอม เริ่มต้นจากระบบทดสอบในสารผสม AlGainP ที่มีโครงสร้างพื้นฐานคล้ายเพชร ระบบ ทดสอบนี้มีจุดเด่นคือระบบประกอบด้วยธาตุหลายชนิดทำให้มีความหลากหลายของพันธะอะตอมขนิดต่าง ๆ ในระบบ เพื่อทดสอบข้อจำกัด ของขนาดของเซลล์หน่วยที่จำเป็นในการศึกษาระบบการเรียงตัวแบบโร้ระเบียบ ผลที่ได้ให้แนวทางที่เป็นประโยชน์ในการวิเคราะห์แนวใน้ม ของคุณสมบัติวัสดุได้จากเซลล์ที่มีขนาดเล็ก ช่วยให้ประหยัดเวลาในการคำนวณและเพิ่มประสิทธิภาพในการสร้างแบบจำลองโครงสร้าง [ตีพิมพ์ในวารสาร Comp. Mater. Sci. 49, S114 (2010)] เมื่อได้เงื่อนไขที่เชื่อถือได้จึงเริ่มศึกษาระบบที่มีการจำกัดมิติเพื่อปรับเปลี่ยน คุณสมบัติของคาร์บอนที่มีความหนาเพียงหนึ่งชั้นอะตอม เรียกว่า แกรฟืน (graphene) ซึ่งวงการวิจัยทั่วโลกให้ความสนใจอย่างมาก (เห็นได้ จากการประกาศผลรางวัลโนเบลปี 2010 ในเดือนตุลาคม 2553) จึงได้ทำการศึกษาการปรับเปลี่ยนคุณสมบัติของแกรฟืนด้วยการสร้างพันธะ ที่แตกต่างกันในแกรฟินโดยการผสมกับโบรอนไนไตรด์ ได้แนวโน้มแบบจำลองโครงสร้างที่มีความเป็นไปได้สูงที่สารทั้งสองจะแยกตัวกันพร้อม ทั้งได้เงื่อนไขโครงสร้างในการผีที่สารผสมกัน จากโครงสร้างที่ได้พบว่าคุณสมบัติทางไฟฟ้าขึ้นกับสมมาตรของโครงสร้างและชนิดของพันธะใน วัสดุอย่างมาก (ส่งเพื่อตีพิมพ์ในวารสาร Phys. Rev. B) ในขั้นตันโครงการนี้ได้สร้างความเข้าใจมากกว่าระบบที่มีการเรียงตัวในระยะสั้นซึ่ง ต้องวิจัยต่อไป เมื่อทราบลักษณะโครงสร้างของสารที่โร้ระเบียบควบคู่กับผลการทดลองจะช่วยให้นักวิจัยเข้าใจความสมพันธ์ของโครงสร้างขึ้น ต้องวิจัยต่อไป เมื่อทราอักษณะโครงสร้างขึ้น

Abstract

Amorphous carbon is a non-crystalline form of carbon consisting of a network of random bonds between carbon atoms. One of a well-known metastable form is diamond-like carbon (DLC) which contains significant amounts of sp³ bonds. The sp³ bonds play a crucial role on the properties of DLC. The fact that DLC contains a significant amount of the sp³ bonds makes its properties appears to be similar to diamonds. For example, it has a wide band gap with optical transparency in the visible region. It has high mechanical hardness and is chemical inert. Presently, the fundamental research on amorphous carbon or short-range ordered system can be considered lacking. More work is needed in order to extend the understanding on short-range ordered system as well as amorphous in general. From the theoretical point of view, the study of non-crystalline material is a bigger challenge in comparison with crystalline materials because the complexity of the atomic disordering and the randomness. The efficient structural model is needed for the study. Since the microscopic structure is not well-defined, the procedure for generating the test structures is important. Moreover, several calculating techniques will be needed in order to bring the theoretical results to compare with experimental observable quantities. The later is needed so that the most probable structural model can be identified. Once the model is identified, it can be used as a starting point to study the role of hybridized bonds as well as effects from impurities.

In this project, we focused our attentions on the structural analysis of carbon-related materials using first-principles calculation (also known as *ab initio* calculations). In the beginning, we studied how microscopic structures (i.e., bonding network and atomic arrangement) affect the properties of materials. The AlGaInP alloy in Zincblende structure, which almost analogous to diamond structure, was used as a test case for studying the size of structural model and electronic properties in short-range ordered system. The results suggested an approximate size of unit cell to acquire a general trend on the electronic properties for system with short-range order [Comp. Mater. Sci. 49, S114 (2010)]. With this confident, we applied the method to study the modification of single layer of carbon atom called "graphene" with boron nitride (BN) compound [submitted for publication in Phys. Rev. B]. At this step, this project presents a better understanding of structural model for non-crystalline or amorphous systems. The atomic randomness in amorphous system is more complicate than short-range ordered structure and subject for further works. Once the model is created various measurable properties can be simulated and compare with different measurement techniques. In conjunction with experimental data, we can extend our current understand on the microscopic structures and properties of materials in wider aspects.

Executive Summary

1. ชื่อโครงการ

โครงสร้างระดับจุลภาคและคุณสมบัติของคาร์บอนคล้ายเพชร Microscopic structures and properties of diamond-like carbon (DLC)

- 2. ชื่อหัวหน้าโครงการและคณะ
 - อ. ดร.สิริโชค จึงถาวรรณ และ ศ. ดร.ชูกิจ ลิมปิจำนงค์
 - Dr. Sirichok Jungthawan and Prof. Dr. Sukit Limpijumnong
- 3. ระยะเวลาดำเนินงาน
 - 2 ปี (16 มีนาคม 2552 ถึง 15 มีนาคม 2554)
- 4. งบประมาณโครงการ

280.000 บาท

5. สถานที่ติดต่อ

สาขาวิชาฟิสิกส์ มหาวิทยาลัยเทคโนโลยีสุรนารี นครราชสีมา 30000 โทร. 044224538, 0869040242 โทรสาร 044224538

e-mail: sirichok@gmail.com, sirichok@sut.ac.th

- 6. วัตถุประสงค์โครงการ
 - 1. ศึกษาโครงสร้างอะตอมและคุณสมบัติของวัสดุโดยวิธีแบบเฟิร์สพรินซิเพิล (First-principles calculation)
 - 2. ศึกษาผลของโครงสร้างที่มีต่อคุณสมบัติของวัสดุจากโครงสร้างอิเล็กทรอนิกส์
 - 3. ศึกษาผลของสารเจือที่มีต่อคุณสมบัติของวัสดุ

7. เนื้อหางานวิจัย

ในขั้นแรกของงานวิจัยนี้เป็นความพยายามในการสร้างแบบจำลองอะตอมที่มีการจัดเรียงตัวแบบไร้ ระเบียบในโครงสร้างคล้ายเพชร (zincblende) โดยการศึกษาโครงสร้างกว่าห้าพันโครงสร้าง เพื่อศึกษาผลของการจัดเรียง ในแบบต่าง ๆ กับคุณสมบัติเชิงอิเล็กทรอนิกส์และศึกษาโครงสร้างแถบพลังงานกับรูปแบบการจัดเรียงของสารในระบบ ซึ่ง เทคนิคในขั้นแรกยังคงตั้งอยู่บนพื้นฐานของโครงสร้างที่คล้ายคลึงกับโครงผลึกของเพชรที่ประกอบด้วยพันธะเคมีแบบ sp³ แต่มีการจัดเรียงตัวของอะตอมแตกต่างกันไป พบว่าคุณสมบัติของวัสดุสามารถทำนายอย่างคร่าว ๆ ได้จากเซลล์หน่วยที่มี ขนาดเล็ก ทำให้ช่วยเพิ่มประสิทธิภาพในการคำนวณ โดยผลการศึกษาได้ตีพิมพ์ในวารสาร Comp. Mat. Sci. (JIF=1.522)

จากผลในขั้นแรก ได้ศึกษาคุณสมบัติของระบบคาร์บอนสองมิติ (แกรฟัน) ซึ่งกำลังเป็นที่สนใจอย่างมากใน วงการวิจัย โดยศึกษาคุณสมบัติของคาร์บอนที่เปลี่ยนไปเมื่อมีการเจือด้วยสารโบรอนไนไตรด์ ซึ่งโครงสร้างของสารนี้ได้มี นักวิจัยทำนายไว้ตั้งแต่ปี 1989 และใช้เรื่อยมาจนถึงปัจจุบัน งานวิจัยชิ้นนี้ได้เสนอแนวคิดของโครงสร้างสารผสมใหม่ที่ นักวิจัยต่างมองข้ามไปกว่า 22 ปี โดยสารดังกล่าวจะพยายามเรียงตัวเป็นโครงสร้างที่มีพันธะแบบ sp² และสารโบรอนไน ไตรด์จะพยายามแยกตัวออกจากคาร์บอนทำให้เกิดเป็นโดเมนของสารบนแผ่นแกรฟัน ผลที่ได้น่าสนใจอย่างมากในการ ปรับเปลี่ยนโครงสร้างของแกรฟินโดยใช้แถบโบรอนไนไตรด์ที่เกิดขึ้นเองจากการแยกตัวออกของสารทั้งสอง ซึ่งอาจเป็นวิธี หนึ่งในการควบคุมคุณสมบัติของสารได้ โดยผลการศึกษาได้ส่งเพื่อพิจารณาตีพิมพ์ในวารสาร Phys. Rev. B (JIF=3.475)

สำหรับโครงสร้างของสารที่ไม่เป็นผลึกและมีการเรียงตัวแบบสุ่มนั้น สามารถสร้างแบบจำลองเริ่มต้นจาก การจัดเรียงตัวแบบสุ่มด้วยเงื่อนไขที่อะตอมแต่ละตัวมีระยะห่างจากกันมากที่สุด และมีความหนาแน่นของระบบใกล้เคียง สารจริง โดยสามารถคำนวณหาสถานะพื้นของโครงสร้างได้แต่เนื่องจากโครงสร้างในธรรมชาติไม่ใช่โครงสร้างที่เรียงตัวแบบ สุ่มโดยสมบูรณ์ เพราะโครงข่ายของอะตอมในสารมีแนวโน้มในการรักษาลักษณะพันธะของระบบ การศึกษาโครงสร้างที่ไม่ เป็นผลึกจึงต้องเริ่มจากโครงสร้างที่สมบูรณ์แล้วค่อยทำลายความเป็นผลึกด้วยการสลับและย้ายตำแหน่งของอะตอมต่าง ๆ โดยอยู่ภายใต้เงื่อนไขที่ระบุอัตราส่วนของพันธะแบบ sp² และ sp³ ที่ผสมกันอยู่ เพื่อความน่าเชื่อถือในการคำนวณ คุณสมบัติของระบบ เช่น จำนวนพันธะและความหนาแน่นสถานะอิเล็กตรอน จำเป็นต้องทำการคำนวณโครงสร้างจำนวน มากเพื่อทำการวิเคราะห์เชิงสถิติที่มีความซับซ้อนมาก หัวข้อนี้จึงอยู่ระหว่างดำเนินการ คาดว่าวิธีในการสร้างแบบจำลอง ของโครงสร้างที่ไม่เป็นผลึกจะช่วยให้สามารถวิเคราะห์คุณสมบัติของสารได้อย่างชัดเจนมากขึ้นกว่าการประมาณที่ใช้กันอยู่ ในปัจจุบัน จะทำให้ทราบแนวทางในการปรับเปลี่ยนคุณสมบัติของสารและพื้นผิวสำหรับการประยุกต์ศึกษาวิจัยในแง่มุมอื่น ต่อไป

8. ผลลัพธ์ที่ได้จากโครงการและกิจกรรม

ผลงานตีพิมพ์ 1 เรื่อง และอยู่ระหว่างพิจารณาตีพิมพ์ 1 เรื่อง

- 1. <u>Sirichok Jungthawan*</u>, Kwiseon Kim, and Sukit Limpijumnong, *The effects of unit cell size on the bandgap range in the direct enumeration study of* Al_xGa_yIn_{1-x-y}P, Comp. Mater. Sci. 49, S114 (2010). [JIF=1.522]
- Sirichok Jungthawan*, Sukit Limpijumnong, and Jer-Lai Kuo, Electronic structures of graphene/boron nitride sheet superlattices, Phys. Rev. B (submitted). [JIF=3.475] เสนอผลงานในการประชุมวิชาการนานาชาติ 4 ครั้ง
- 1. <u>Sirichok Jungthawan</u> and Jer-Lai Kuo, *Structural stability and electronic structure of monolayer* BC₂N *ordered structures*, The 13th Asian Workshop on First-Principles Electronic Structure Calculations (1–3 Nov 2010), POSTECH, Pohang, KOREA
- 2. <u>Sirichok Jungthawan</u> and Jer-Lai Kuo, *Structural stability and electronic structure of monolayer* BC₂N *ordered structures*, 10th Workshop on First-Principles Computational Materials Physics (21–23 Jul 2010), Taitung, TAIWAN
- 3. <u>Sirichok Jungthawan</u>, Kwiseon Kim, and Sukit Limpijumnong, *The effects of unit cell size on the bandgap range in the direct enumeration study of AlGaInP alloys*, 2010 Annual Meeting of Asian CORE Program (1–2 Mar 2009), Taipei, TAIWAN
- 4. <u>Sirichok Jungthawan</u>, Kwiseon Kim, Peter Graf, and Sukit Limpijumnong, *Direct enumeration studies of band–gap properties of AlGaInP alloys*, ICMAT 2009 (28 Jun–3 Jul 2009), SINGAPORE

วิทยากรรับเชิญ 1 ครั้ง

1. Invited speaker on EXAFS analysis by Artemis software, 2nd Workshop on X–ray Absorption Spectroscopy (Jun 2009), Synchrotron Light Research Institute (SLRI), Nakhon Ratchasima, THAILAND

ผู้ดำเนินการประชุมวิชาการนานาชาติ 1 ครั้ง

1. Session Chair in Symposium Q–S11: Materials Modeling at Continuum and Macroscopic Levels, ICMAT 2009 (28 Jun–3 Jul 2009), SINGAPORE

เดินทางทำวิจัยต่างประเทศ 1 ปี (ช่วงมกราคม ถึง ธันวาคม 2553)

1. สถาบัน Institute of Atomic and Molecular Sciences (IAMS), Academia Sinica, Taipei, TAIWAN ในหัวข้อ Theoretical study of structural arrangement at atomic-nanoscale of carbon-based materials and its properties

ภาคผนวก

- 1. ผลงานตีพิมพ์
 - S. Jungthawan*, K. Kim, and S. Limpijumnong, Comp. Mater. Sci. 49, S114 (2010). [JIF=1.522]
- 2. บทความสำหรับการเผยแพร่
- 3. ผลงานที่ส่งเพื่อพิจารณาตีพิมพ์
 - <u>S. Jungthawan*</u>, S. Limpijumnong, and J.-L. Kuo, Phys. Rev. B (submitted). [JIF=3.475]
- 4. เอกสารแสดงการส่งผลงานตีพิมพ์
- 5. บทคัดย่องานประชุมวิชาการนานาชาติ
 - The 13th Asian Workshop on First-Principles Electronic Structure Calculations (1–3 Nov 2010), POSTECH, Pohang, KOREA
 - 10th Workshop on First-Principles Computational Materials Physics (21–23 Jul 2010), Taitung, TAIWAN
 - 2010 Annual Meeting of Asian CORE Program (1–2 Mar 2009), Taipei, TAIWAN
 - ICMAT 2009 (28 Jun-3 Jul 2009), SINGAPORE

ELSEVIER ELSEVIER

Contents lists available at ScienceDirect

Computational Materials Science

journal homepage: www.elsevier.com/locate/commatsci



The effects of unit cell size on the bandgap range in the direct enumeration study of $Al_xGa_vIn_{1-x-v}P$ alloys

Sirichok Jungthawan a,b,*, Kwiseon Kim c, Sukit Limpijumnong a,b

- a School of Physics, Institute of Science, Suranaree University of Technology and Synchrotron Light Research Institute, Nakhon Ratchasima 30000, Thailand
- ^b Thailand Center of Excellence in Physics (ThEP Center), Commission on Higher Education, Bangkok 10400, Thailand

ARTICLE INFO

Article history: Received 8 September 2009 Received in revised form 21 January 2010 Accepted 21 January 2010 Available online 18 April 2010

Keywords: AlGaInP Direct enumeration Ordering Bandgap reduction Bandgap range Band interaction

ABSTRACT

Direct enumeration method is an efficient way for scanning alloy properties by computing all possible configurations. This method thoroughly covers all possible configurations without bias and provides an informative trend of alloy properties on ordering patterns. In an actual study, the number of possible configurations increases rapidly with the size of the unit cell and usually a reasonable size that give a sufficiently large number of configurations are chosen. In this work, the convergence of the bandgap range with respect to the unit cell size of AlGaInP alloy is studied up to 8 cation atoms per unit cell. It is found that the bandgap range already converges to within 0.1 eV when the unit cell size is 4 cation atoms. Interestingly, we also found that the lowest bandgap value of GaInP alloy is achieved already in a small cell (2 cations in the unit cell). The cause for this special small bandgap case is discussed.

© 2010 Elsevier B.V. All rights reserved.

1. Introduction

Alloying provides a flexible way to engineer electronics and optical properties of semiconductors to suit the need of new generation device applications [1–3]. The properties of semiconductor alloys, especially those of III-V alloys, have been extensively studied in the last decade [1-4]. Several schemes were proposed to explain the relationship between the properties and the alloy composition. The simplest and most known scheme (the Vegard's rule) assumes a linear dependence between the interested property and the alloy composition [5,6]. In reality, most properties are not linearly dependent with the alloy composition. As a result, non-linear terms have been proposed to quantify the deviation from the Vegard's trend. The most known improved scheme added a bowing parameter [7]. However, neither the Vegard's rule nor its variants takes into account the ordering of the constituent atoms in the alloy. It is important to note that, for a given alloy composition. there are virtually infinite possible arrangements of the atoms in the alloy. From the theoretical point of view, the direct enumeration method (DEM) has been used to study alloy systems [8-11]. The important elements of the method are the algorithm to gener-

E-mail address: sirichok@sut.ac.th (S. Jungthawan).

ate alloy configurations [10,12,13] and the practical method to calculate their properties [8,10,11,14–17]. The algorithm to generate alloy configurations for binary alloy with face-centered cubic (FCC) and body-centered cubic (BCC) lattice have been proposed by Ferreira et al. [10]. Later, an efficient algorithm for generating alloy configurations has been introduced by Hart and Forcade [18] where the run time scales linearly with the number of distinct configurations. Recently, an algorithm for generating alloy configurations of a non-primitive lattice and application to hexagonal close packed alloys have been developed [19]. The DEM has been used to study the bandgap properties calculated by empirical pseudopotential method (EPM) [14-17,20-23] of several classes of semiconductor alloys; including the ternary [9-11] and quaternary [24] alloys. An advantage of DEM is that it relates the interested property to the alloy configuration (atomic ordering) in additional to the composition. From EPM calculation, we have previously shown that the bandgap of AlGaInP alloy depends strongly on the atomic ordering in addition to the alloy composition [24]. In that work, we have also shown that most of the alloy configurations have the bandgaps that are smaller than the values predicted by the Vegard's rule. The ordering causes a reduction in the bandgap; pushing it below the Vegard's trend [24-26]. The lowering of the bandgap due to atomic arrangements emphasizes the role of the alloy configurations (in addition to the alloy composition) in bandgap engineering. In this work and our previous work [24], we focused our attentions in studying a complete set of theoretical

^c National Renewable Energy Laboratory, Golden, Colorado 80401, USA

^{*} Corresponding author at: School of Physics, Institute of Science, Suranaree University of Technology and Synchrotron Light Research Institute, Nakhon Ratchasima 30000, Thailand. Tel.: +66 44224319; fax: +66 44224651.

possible arrangements within a given cell size. These complete results allow us to investigate how the band properties relate to the atomic arrangements. However, we should keep in mind that many of the configurations studied might have a very high energy and difficult to fabricate.

Because there are many distinct alloy configurations for a given alloy composition, DEM gives the possible range of properties (for e.g., the bandgap and the electron effective mass) at a given alloy composition, as well as the relationship between the ordering and a given property. While a larger cell size gives more possible configurations (allowing a more complete study) and finer composition steps, the computational demand is increased rapidly. Therefore, it is important to investigate the size of unit cell that sufficiently gives the converged results. In this work, we focus on the quaternary alloys $Al_xGa_yIn_{1-x-y}P$ (also called pseudoternary alloys that contain three mixed-cations in the FCC sublattice).

2. Calculation

The alloy configurations of AlGaInP are generated by applying DEM [9,11,24] to a zincblende-based alloy system. The possible number of alloy configurations for a unit cell containing N cation atoms is given by the multichoose formula [27], $\binom{n+N-1}{N}$ (n-1,N)!, with n being the number of elements. For AlGaInP alloy, n = 3. A subroutine in the Alloy Theoretic Automated Toolkit (ATAT) package [28,29] was employed to systematically generate the configurations. The detail of alloy configurations generated by ATAT is described elsewhere [24]. Note that, some of the generated configurations are equivalent by symmetries and the redundant configurations were removed to reduce computation demand. Using the ATAT codes, the cell size of up to 8 cation atoms per unit cell ($N_{\text{max}} = 8$) provides a total of 9808 distinct configurations. They are composed of 1887 pseudobinary alloy configurations from the three parent binary compounds (3 × 629 AlGaP, GaInP and AlInP) and 7918 pseudoternary alloy configurations [see Ref. [24] (Table 1) for detail].

Because the composition of the $Al_xGa_yIn_{1-x-y}P$ alloys is defined by two variables (x and y), the composition space can be presented in a two-dimensional space. We have previously shown that the two-dimension composition space of this ternary alloy system is well described by using the transformed coordinates, u = x + y/2 and $v = \sqrt{3}y/2$ [24]. This leads to a regular triangle, as shown in Fig. 1. The parent compounds are located at the vertices and the circles represent the alloy compositions that can be obtained by each unit cell size.

To reduce the computation demand, alloy properties of all generated configurations are calculated by using EPM [14,15]. The structural relaxation was done by the valence force field method (VFF) [30–33]. In EPM, the electronic structures are obtained by solving the simplified Schrödinger equation

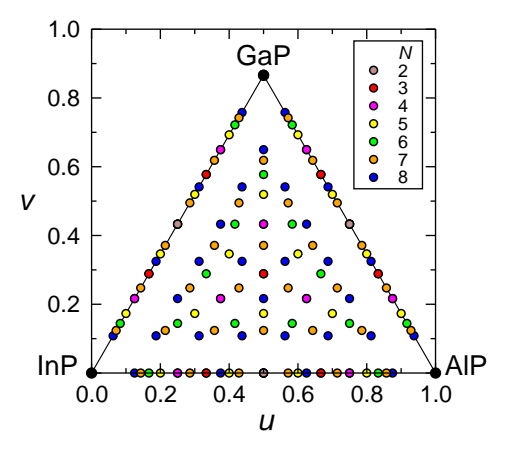


Fig. 1. The composition space of the pseudoternary alloy system. The colored circles show the possible compositions given by each unit cell size (i.e. N = 2, 3, 4, 5, 6, 7, and 8). Circles on the three edges of the triangle correspond to the pseudobinary alloys.

$$\left\{ -\frac{1}{2} \nabla^2 + \sum_{\alpha,n} V_{\alpha}(\mathbf{r} - \mathbf{R}_{\alpha,n}) \right\} \psi_i(\mathbf{r}) = \varepsilon_i \psi_i(\mathbf{r})$$
 (1)

where the effective pseudopotential is summed over all individual atoms n (α denotes atomic type). V_{α} is the screened potential for atomic type α and $\mathbf{R}_{\alpha,n}$ is the atomic position of atom n (type α) obtained after VFF relaxations. One advantage of EPM (over first-principles density functional calculations) is that it provides the bandgaps that do not need corrections. This is because the parameters are already fitted to the experimental bandgaps. The cutoff energy of the generated pseudopotentials is 68 eV. The details of the fitting parameters for the atomic potentials of AlP, GaP, and InP compounds can be found in Ref. [16]. Details of EPM method [14–16] and electronic structure computation are described elsewhere [24].

For each set of the configurations in a unit cell size, the maximum and the minimum bandgaps are determined. The possible range of bandgaps is the difference between the maximum and the minimum values at a given composition. Because the ordering of cation atoms can cause a bandgap reduction [24], the larger cell size, which facilitates more degree of ordering, is likely to provide a smaller minimum bandgap than the smaller cell size. However, it is expected that the minimum value of bandgap would converge at a sufficiently large cell. In this work, the largest cell size used is the unit cell with 8 cations. The bandgap minima are calculated for cell size of, $N_{\rm max}$ = 4, 5, 6, 7, and 8. The upper bound of bandgap is set by the Vegard's rule which represent the disordered alloys [24]. According to Vegard's rule, the (upper bound) bandgap of Al_{x-} Al_{x-}

$$E_{\rm gap}(x,y) = xE_{\rm gap}(AlP) + yE_{\rm gap}(GaP) + (1-x-y)E_{\rm gap}(InP) \tag{2} \label{eq:gap}$$

Table 1The selected alloy configurations with ordering in the [1 1 1] directions. Only the positions of the cations are listed (the position of P atoms are shifted by (0.25, 0.25, 0.25) from the cation positions). The lattice vectors and the cation positions are in the Cartesian coordinates in the unit of lattice constant.

Alloy configuration	Lattice vector	Cation position	Alloy ordering
I	(-0.5, 0.5, 1) (-0.5, 1, 0.5) (-1, 0.5, 0.5)	Ga: (-2, 2, 2) In: (-1, 1, 1)	$(GaP)_1 (InP)_1$
II	(-1.5, 1, 1.5) (-1, 1.5, 1.5) (-1.5, 1.5, 1)	Ga: (-1, 1, 1), (-4, 4, 4) In: (-2, 2, 2), (-3, 3, 3)	$(GaP)_2 (InP)_2$
IIIa	(-0.5, 0, -0.5) (0, -0.5, 0.5) (-2, 2, 2)	Ga: (-0.5, 0, 0.5), (-1, 0.5, 0.5), (-2.5, 1.5, 2) In: (-1.5, 0.5, 1), (-1.5, 1, 1.5), (-2, 1.5, 1.5)	$(GaP)_3 (InP)_3$
IIIb	(-0.5, 0, -0.5) (0, -0.5, 0.5) (-2, 2, 2)	Ga: (-0.5, 0, 0.5), (-1.5, 0.5, 1), (-2.5, 1.5, 2) In: (-1, 0.5, 0.5), (-1.5, 1, 1.5), (-2, 1.5, 1.5)	$(GaP)_1 (InP)_1 (GaP)_2 (InP)_2$
IV	(-2.5, 2.5, 3) $(-2.5, 3, 2.5)$ $(-3, 2.5, 2.5)$	Ga: (-1, 1, 1), (-3, 3, 3), (-6, 6, 6), (-8, 8, 8) In: (-2, 2, 2), (-4, 4, 4), (-5, 5, 5), (-7, 7, 7)	(GaP) ₄ (InP) ₄

Table 2The calculated bandgap deformation coefficients and the interaction potential V_L for the alloy configurations in Table 1. The values in the parentheses are the experimental values of the coefficients reported in Ref. [41].

Configuration	E(0) (eV)	α (meV/GPa)	β (meV/GPa ²)	V_L (eV)
InP	$E_{\Gamma} = 0.525$ $E_{I} = 1.362$	74.1 34.7	-1.71 -0.80	-
GaP	E_{Γ} = 1.822	89.7	-1.44	-
Disordered	$E_L = 1.616$ $E_T = 1.173$	34.9 81.9 (92)	-0.62 -1.57 (-3.3)	_
Ga _{0.5} In _{0.5} P	$E_L = 1.489$	34.8 (43)	-0.71	
I II	$E_{-} = 0.625$ $E_{-} = 0.708$	57.3 65.8	−1.47 −1.70	0.71 0.60
IIIa IIIb	$E_{-} = 0.762$ $E_{-} = 0.657$	55.9 58.9	-0.80 -1.95	0.56 0.68
IV	$E_{-} = 0.662$	50.3	-3.14	0.67

where $E_{\rm gap}({\rm AlP})$, $E_{\rm gap}({\rm GaP})$, and $E_{\rm gap}({\rm InP})$ are the bandgaps of AlP, GaP, and InP, respectively. These bandgap values from EPM calculation along with the corresponding experimental values are given in Ref. [24] (Table 2). The convergence of bandgap range is studied by calculating the possible range of bandgaps as the cell size increased. Because the possible alloy composition of each cell-size is discrete in the composition space, a third-degree polynomial function of the form

$$\Delta E_{\text{gap}} = a + bx + cy + dx^{2} + ey^{2} + fxy + gx^{3} + hy^{3} + ixy^{2} + jx^{2}y$$
(3)

is used to fit the calculated bandgap range by the least square method to generate fine-mesh data points for the contour plots. The contour plots of bandgap range for different $N_{\rm max}$ used are shown in Fig. 2. Note that the bandgap range at all three vertices are zero because there is only one possible configuration at those points.

3. Results and discussion

The ordering in the crystal structure induces the band interactions that can lower the bandgap. Because a larger cell size provides more degree of freedom of ordering, new configurations with lower bandgaps are expected as the cell size used in DEM is increased. The lowering of the minimum bandgap leads to the wider possible bandgap range. However, the range of the bandgaps is expected to converged (within a reasonable tolerance) with the cell size. The calculated bandgap range for each limited cell size as a function of alloy composition is shown in Fig. 2. We can see that the bandgap range is quite large (up to 0.8 eV) for the compositions near the middle of the composition space (slightly shifted toward the low Al composition side). The bandgap range is reduced as we move toward the vertices and goes to zero at the vertices. By visual observation, we can already see that the contour plots of the bandgap range for N_{max} = 5 and above are quite similar. The polynomial function for the contour plot of the largest cell size $(N_{\text{max}} = 8)$ is given by

$$\Delta E_{\text{gap}} = 2.34x + 4.12y - 3.18x^2 - 6.98y^2 - 5.27xy + 0.84x^3$$
$$+ 2.85y^3 + 2.36xy^2 + 1.32x^2y$$
 (4)

where the bandgap reduction ($\Delta E_{\rm gap}$) is in eV and x, y are the alloy compositions of ${\rm Al}_x{\rm Ga}_y{\rm In}_{1-x-y}{\rm P}$.

To qualitatively determine the convergence of the bandgap ranges as a function of cell size, we compute the difference between the bandgap ranges of each $N_{\rm max}$ with those of the largest cell used ($N_{\rm max}$ = 8). This is done by calculating the average rootmean-square of the difference (Δ). The average is done over the entire composition space. First, a 200 × 200 uniform mesh in the composition space is created. Then, at each point in alloying composition (total of 20,301 points), the bandgap range for each $N_{\rm max}$ is calculated from the polynomial fitted function. The root-mean-

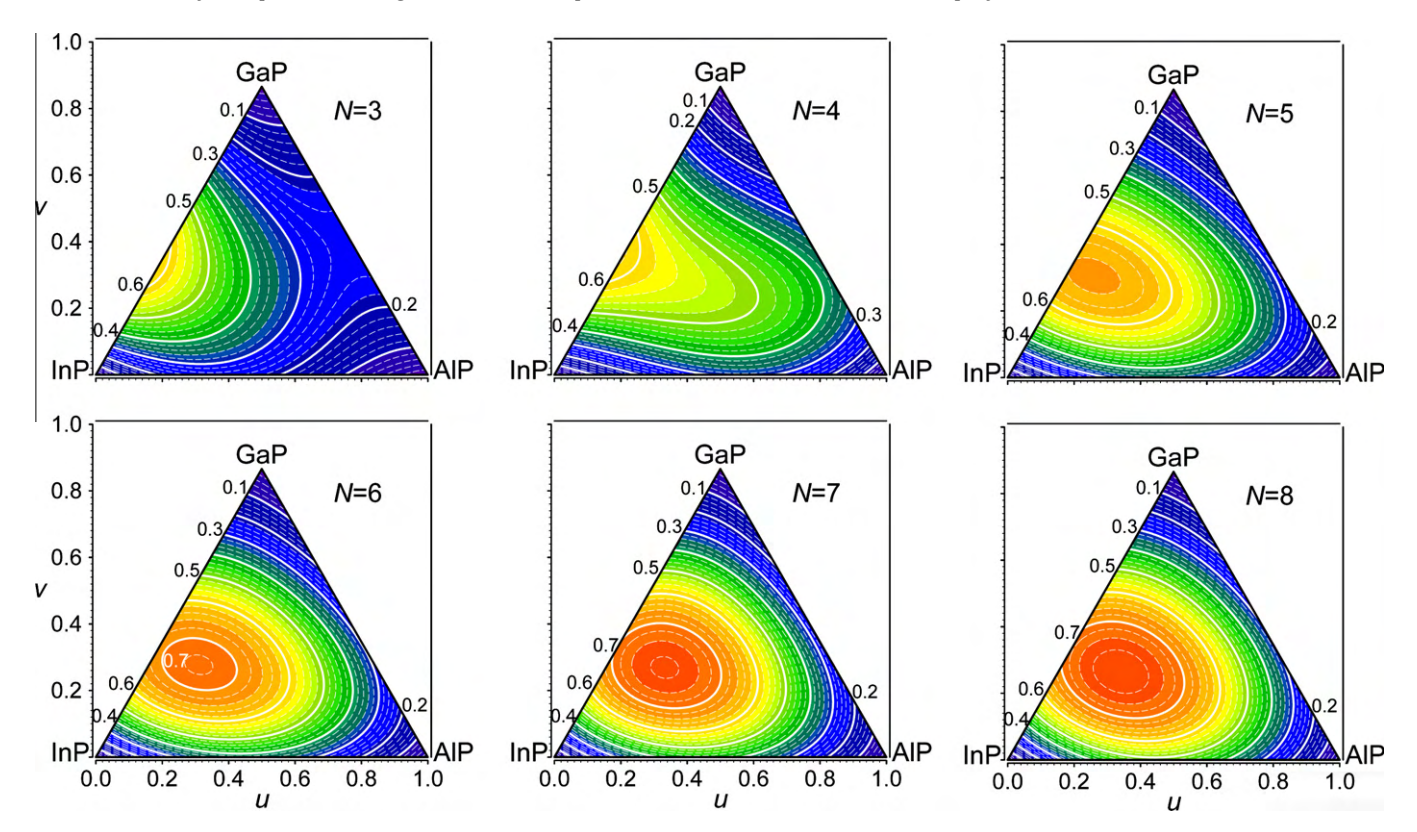


Fig. 2. The contour plots of the calculated bandgap ranges of pseudoternary AlGalnP as a function of alloy compositions (u = x + y/2 and $v = \sqrt{3}y/2$). Each figure shows the results of the calculation with a different N_{max} . Note that a third-degree polynomial function is used to fit to the calculated data, in order to generate the fine-mesh data for the plots.

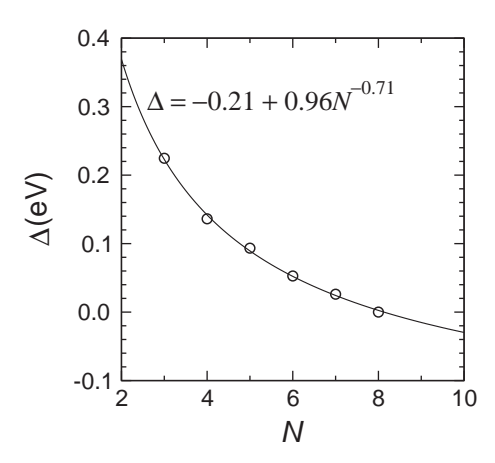


Fig. 3. The root-mean-square difference (Δ) of bandgap range for each cell sizes (N_{max}), with respect to $N_{\text{max}} = 8$. The curve represents the fit to the data.

square of the difference (between that of interested $N_{\rm max}$ and that of $N_{\rm max}$ = 8) in bandgap range is calculated and the average (Δ) over all mesh points are calculated. In Fig. 3, Δ as a function of $N_{\rm max}$ along with the function (in the form of Δ = a + bN^c) is shown. It is found that Δ started to converge (with the tolerant of \sim 0.1 eV referenced to the $N_{\rm max}$ = 8 calculation) already at the cell size containing 5 cation atoms.

For pseudobinary alloys, AlGaP tends to have a rather large bandgap range of \sim 0.5 eV (see Fig. 2 for $N_{\rm max}$ = 8). AlInP has an even larger bandgap range of ~0.6 eV. For GaInP, it is interesting that the large bandgap range of \sim 0.6 eV is already observed at a small cell N_{max} = 3. This indicates that an ordering that can significantly reduce the bandgap of GaInP alloy can be represented by a small cell size. It has been found that the ordering in [1 1 1] direction of the CuPt ordered structure can give a large bandgap reduction [9,24]. The crystal parameters of CuPt ordered structure consisting of 2 cations/cell is shown in Table 1. In general, we can expect more degree of freedom in ordering to give an increased bandgap range. As a result, the smaller bandgap configuration would occur in the large cell size. However, for this special case, the bandgap of GaInP reduction of CuPt ordered structure provides the minimum bandgap value for the 50% alloy (Ga_{0.5}In_{0.5}P). This occurs because the conduction state that folded onto the Γ point (from the L point) interacts strongly with the conduction band minimum at the Γ point. Because the folding that causes this interaction already took place in the small cell, increasing cell size (allow more flexibility of orderings) does not make the interaction stronger for this particular case. As a result, the bandgap range at this composition converges at a small cell size. To further investigate the band interaction for this particular case, first-principles calculations are performed.

We employed first-principles calculations to examine the electronic structures of several selected configurations ordering in the [1 1 1] direction. The crystal parameters and atomic coordinates of these configurations are shown in Table 1. The calculations were performed by the ultrasoft pseudopotential approach with the projector augmented wave (PAW) method [34,35] and a plane wave basis set (324 eV cutoff) as implemented in the VASP code [36–38]. The Γ -centered Monkhorst–Pack k-mesh is used for Brillouin zone integration.

To study the bandgap change as a function of pressure, for each of alloy configurations, bandgap at the Γ point is calculated at different volume (V). To relate the volume to the applied pressure, the total energy as a function of volume is fitted with the Rose equation of states [39]. For each configuration, the pressure dependence of bandgap (at Γ) can be described by the relationship

 $E(P) = E(0) + \alpha P + \beta P^2$. The parameters α and β are obtained by the least square fit to the calculated (first-principles) results and tabulated in Table 2. The ordering in the [1 1 1] direction causes the conduction band minimum at L to fold to Γ (called L_{c1}). The nonlinearity of E(P) is a result of the repulsion between the conduction states at Γ and L_{c1} [40]. Because the conduction state is pushed down, the bandgap in this configuration is reduced [25,26]. To study the effects of the interactions, the bandgaps of the ordered structures are compared with that obtained from the Vegard's rule (the linear interpolation between the bandgaps of parent compounds) which represents the case of completely disordered alloy. In Table 2, the bandgap of the disordered alloy is calculated by averaging the bandgaps of parent compounds (GaP and InP). The interaction between Γ and L_{c1} can be described by the first order perturbation theory. The perturbed energies of Γ and L_{c1} can be expressed as [41],

$$E_{\pm} = 1/2 \left[(E_L + E_{\Gamma}) \pm \sqrt{(E_L - E_{\Gamma})^2 + 4V_L^2} \right]$$
 (5)

where E_+ and E_- are the energies of perturbed L_{c1} and Γ states. E_L and E_Γ are the energies of unperturbed Γ and L (obtained by Vegard's rule). If we assumed that the interaction potential (V_L) does not depend on the pressure, V_L can be calculated by fitting each sets of E_- , E_L , and E_Γ to Eq. (5). The values of V_L obtained by the least squares fit are shown in Table 2. The obtained values of V_L clearly show that GaP/InP monolayer superlattice (structure I with N=2) has the strongest interaction ($V_L=0.71$ eV). As a result, the configuration has the largest bandgap reduction among GaInP alloys [42].

4. Conclusions

The convergence of the bandgap range of AlGaInP alloys with respect to the cell size used in the direct enumeration method (DEM) is studied. By directly calculating a large number of alloy configurations, the bandgap range as a function of alloy compositions are determined by DEM using various unit cell size $(N_{\text{max}} = 2-8)$. It is found that it is sufficient to use the cell size with 5 cation atoms (N_{max} = 5). The bandgap range of AlGaInP alloy is reported (in the form of a polynomial function). It is found that the bandgap range is large (~0.8 eV) for the compositions near the middle of the composition space (slightly shifted toward the low Al composition side). In addition to the convergence study, the source of the bandgap reduction of the alloy in the [1 1 1] superlattice configurations are investigated. It is found that the superlattice in this direction has strong interactions between the Γ and the folded L states and the GaP/InP monolayer superlattice has the strong interaction among studied configurations.

Acknowledgements

The work is supported by NANOTEC (Grant No. NN-B-22-DI2-20-51-09), AOARD/AFOSR (Contract No. FA2386-09-1-4106), and DOE (Contract No. DE-AC36-99GO10337). The authors thank L.-W. Wang for providing the PESCAN codes. One of the authors (SJ) acknowledges the funding from the Thailand Research Fund (Grant No. MRG5280235).

References

- [1] A.S. Dissanayake, S.X. Huang, H.X. Jiang, J.Y. Lin, Phys. Rev. B 44 (1991) 13343.
- [2] H.X. Jiang, G. Brown, J.Y. Lin, J. Appl. Phys. 69 (1991) 6701.
- [3] S. Krishnamurthy, A. Sher, M. Madou, A.B. Chen, J. Appl. Phys. 64 (1988) 1530.
- [4] M.F. Ling, D.J. Miller, Phys. Rev. B 38 (1988) 6113.
- [5] L. Vegard, Z. Phys. 5 (1921) 17.
- [6] L. Vegard, Z. Kristallogr. 67 (1928) 239.
- [7] A. Ebina, Y. Sato, T. Takahashi, Phys. Rev. Lett. 32 (1974) 1366.
- [8] A. Franceschetti, A. Zunger, Nature 402 (1999) 60.

- [9] K. Kim, P.A. Graf, W.B. Jones, J. Comput. Phys. 208 (2005) 735.
- [10] L.G. Ferreira, S.H. Wei, A. Zunger, Int. J. High Perform. Comput. Appl. 5 (1991) 34.
- [11] P.A. Graf, K. Kim, W.B. Jones, G.L.W. Hart, Appl. Phys. Lett. 87 (2005) 243111.
- [12] J. Rutherford, Acta Crystallogr. A 51 (1995) 672.
- [13] J. Rutherford, Acta Crystallogr. A 48 (1992) 500.
- [14] L.-W. Wang, A. Zunger, J. Chem. Phys. 100 (1994) 2394.
- [15] A. Canning, L.-W. Wang, A. Williamson, A. Zunger, J. Comput. Phys. 160 (2000) 29.
- [16] T. Mattila, L.W. Wang, A. Zunger, Phys. Rev. B 59 (1999) 15270.
- [17] K.A. Mäder, A. Zunger, Phys. Rev. B 50 (1994) 17393.
- [18] G.L.W. Hart, R.W. Forcade, Phys. Rev. B 77 (2008) 224115.
- [19] G.L.W. Hart, R.W. Forcade, Phys. Rev. B 80 (2009) 014120.
- [20] K.A. Mäder, A. Zunger, Phys. Rev. B 51 (1995) 10462.
- [21] K.A. Mäder, L.-W. Wang, A. Zunger, Phys. Rev. Lett. 74 (1995) 2555.
- [22] A. Franceschetti, A. Zunger, Phys. Rev. B 52 (1995) 14664.
- [23] J. Kim, L.-W. Wang, A. Zunger, Phys. Rev. B 56 (1997) R15541.
- [24] S. Jungthawan, S. Limpijumnong, R. Collins, K. Kim, P.A. Graf, J.A. Turner, J. Appl. Phys. 105 (2009) 123531.
- [25] S.H. Wei, A. Zunger, Appl. Phys. Lett. 56 (1990) 662.

- [26] L.C. Su, I.H. Ho, N. Kobayashi, G.B. Stringfellow, J. Cryst. Growth 145 (1994) 140.
- [27] W. Feller, An Introduction to Probability Theory and its Applications, vol. 1, Wiley, New York, 1968.
- [28] A. vandeWalle, M. Asta, G. Ceder, CALPHAD J. 26 (2002) 539.
- [29] A. van de Walle, G. Ceder, J. Phase Equilib. Diff. 23 (2002) 348.
- [30] P.N. Keating, Phys. Rev. 145 (1966) 637.
- [31] R.M. Martin, Phys. Rev. B 1 (1970) 4005.
- [32] J.L. Martins, A. Zunger, Phys. Rev. B 30 (1984) 6217.
- [33] M.C. Schabel, J.L. Martins, Phys. Rev. B 43 (1991) 11873.
- [34] P.E. Blöchl, Phys. Rev. B 50 (1994) 17953.
- [35] G. Kresse, D. Joubert, Phys. Rev. B 59 (1999) 1758.
- [36] G. Kresse, J. Furthmüller, Comput. Mater. Sci. 6 (1996) 15. [37] G. Kresse, J. Furthmüller, Phys. Rev. B 54 (1996) 11169.
- [38] G. Kresse, J. Hafner, J. Phys.: Condens. Matter 6 (1994) 8245.
- [39] J.H. Rose, J.R. Smith, F. Guinea, J. Ferrante, Phys. Rev. B 29 (1984) 2963.
- [40] T. Kobayashi, M. Ohtsuji, S. Deol, J. Appl. Phys. 74 (1993) 2752.
- [41] J. Dong, Z. Wang, D. Lu, X. Liu, X. Liu, D. Sun, Z. Wang, M. Kong, G. Li, Appl. Phys. Lett. 68 (1996) 1711.
- [42] S.R. Kurtz, J. Appl. Phys. 74 (1993) 4130.

The effects of unit cell size on the bandgap range in the direct enumeration study of $Al_xGa_vIn_{1-x-v}P$ alloys

ผลกระทบของขนาดเซลล์หน่วยในแบบจำลองโครงสร้างกับช่วงของแถบพลังงานในสารผสม AlGainP

Sirichok Jungthawan^{a,b,*}, Kwiseon Kim^c, Sukit Limpijumnong^{a,b} สิริโชค จึงถาวรรณ Kwiseon Kim และ ชูกิจ ลิมปิจำนงค์

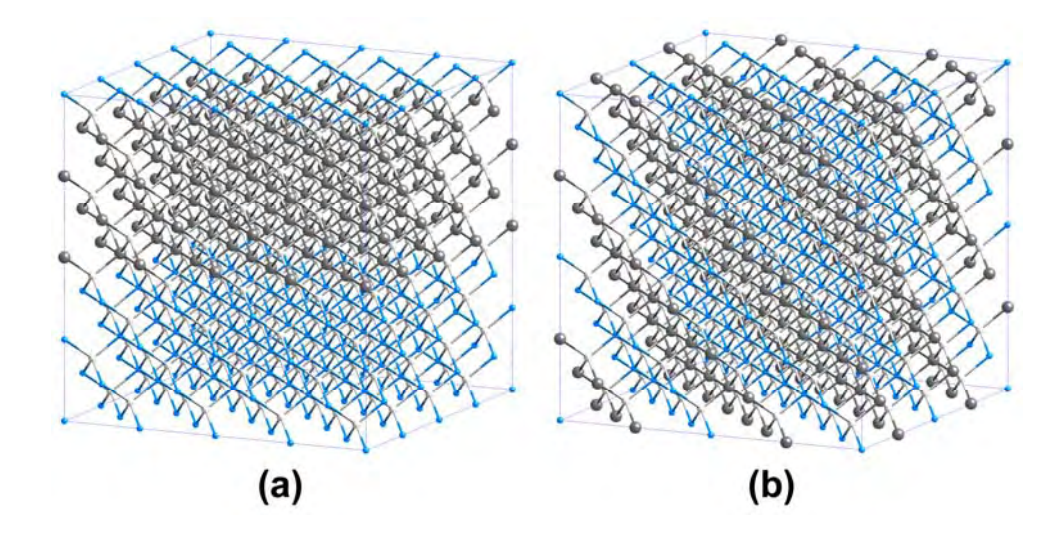
- [°] School of Physics, Institute of Science, Suranaree University of Technology and Synchrotron Light Research Institute, Nakhon Ratchasima 30000, Thailand สาขาวิชาฟิสิกส์ สำนักวิชาวิทยาศาสตร์ มหาวิทยาลัยเทคโนโลยีสุรนารี และ สถาบันวิจัยแสงซินโครต รอน นครราชสีมา 30000 ประเทศไทย
- ^b Thailand Center of Excellence in Physics (ThEP Center), Commission on Higher Education, Bangkok 10400, Thailand ศูนย์ความเป็นเลิศด้านฟิสิกส์ สำนักงานคณะกรรมการการอุดมศึกษา กรุงเทพมหานคร 10400 ประเทศไทย

สารกึ่งตัวนำเป็นวัสดุสำคัญในชิ้นส่วนของอุปกรณ์ต่าง ๆ ที่เกี่ยวข้องกับเทคโนโลยีในปัจจุบัน โดยการประยุกต์ใช้งานจากคุณสมบัติเชิงไฟฟ้าและแสงของสาร การสังเคราะห์สารให้มีคุณสมบัติตาม ต้องการเป็นหัวข้อสำคัญในการพัฒนาอุปกรณ์สำหรับการประยุกต์ใช้ในด้านต่าง ๆ เช่น พลังงาน ทดแทน การอ่านและเก็บข้อมูลด้วยแสง และเทคโนโลยีเลเซอร์ เป็นต้น การปรับคุณสมบัติของสารกึ่ง ตัวนำจะใช้การผสมสารที่มีคุณสมบัติต่างกันในอัตราส่วนผสมต่าง ๆ เพื่อสังเคราะห์สารใหม่ให้มี คุณสมบัติตามต้องการ หรือลดต้นทุนโดยการใช้สารที่ราคาถูกกว่าแทนสารที่มีราคาแพงแต่ให้ คุณสมบัติใกล้เคียงกัน การผสมสารหลาย ๆ ชนิดช่วยเพิ่มตัวแปรในการควบคุมคุณสมบัติของสาร เช่น สารผสมแบบสองธาตุ ได้แก่ ZnO และ SiC แบบสามธาตุ ได้แก่ AlGaAs GaInP และ GaInN และแบบสี่ธาตุ ได้แก่ AlGaInP AlGaInN

โดยทั่วไปการทำนายคุณสมบัติกับอัตราส่วนผสมจะใช้การประมาณแบบเชิงเส้น ซึ่งใช้ได้ดีกับ คุณสมบัติเชิงกลแต่ใช้ไม่ได้กับคุณสมบัติอื่น ๆ ที่ขึ้นกับโครงสร้างของอิเล็กตรอนในเนื้อสาร เช่น คุณสมบัติเชิงไฟฟ้าและแสง จึงเป็นที่มาของโจทย์วิจัยเนื่องจากคุณสมบัติสารผสมมีความสัมพันธ์ที่ไม่ แน่นอนระหว่างคุณสมบัติกับอัตราส่วนผสม เช่น ผสมสารด้วยอัตราส่วนที่เท่ากันแต่กระบวนการ สังเคราะห์ที่ต่างกันก็ทำให้คุณสมบัติเปลี่ยนไปด้วย ซึ่งเป็นความยุ่งยากที่ตามมาในสารผสม ทั้งนี้ยังไม่ มีการศึกษาอย่างลึกซึ้งว่าคุณสมบัติขึ้นกับอัตราส่วนผสมและปัจจัยอื่นอย่างไรบ้าง ทำให้การ สังเคราะห์สารที่มีคุณสมบัติตามต้องการทำได้ยากและซับซ้อน

งานวิจัยนี้จึงมุ่งพัฒนาระเบียบวิธีการคำนวณพร้อมสร้างแบบจำลองเพื่อใช้ทำนายและศึกษา
คุณสมบัติของสารกึ่งตัวนำ เพื่อออกแบบคุณสมบัติของสารจากการเรียงตัวของอะตอมและโครงสร้าง
จุลภาคที่เป็นหน่วยย่อยที่สุดในเนื้อวัสดุ เป็นแนวทางที่จะช่วยให้เกิดการพัฒนาในอุปกรณ์เชิงแสง
และอุปกรณ์เทคโนโลยีขั้นสูง ทั้งนี้ระเบียบวิธีคำนวณที่พัฒนาขึ้นสามารถประยุกต์ใช้กับวัสดุอื่น ๆ ได้
ด้วย เช่น โลหะผสม วัสดุแม่เหล็ก ฯลฯ โดยวิทยานิพนธ์นี้ศึกษาผลของการจัดเรียงตัวในโครงสร้าง
จุลภาคและอัตราส่วนผสมที่มีต่อคุณสมบัติของสารโดยมุ่งเน้นที่การจัดเรียงตัว เพราะสารที่อัตรา

^c National Renewable Energy Laboratory, Golden, Colorado 80401, USA



ส่วนผสมเท่ากันอาจจะเรียงตัวได้ต่างกัน การเรียงตัวจึงเป็นตัวแปรที่สำคัญมากที่มีผลต่อคุณสมบัติ โดยรวม

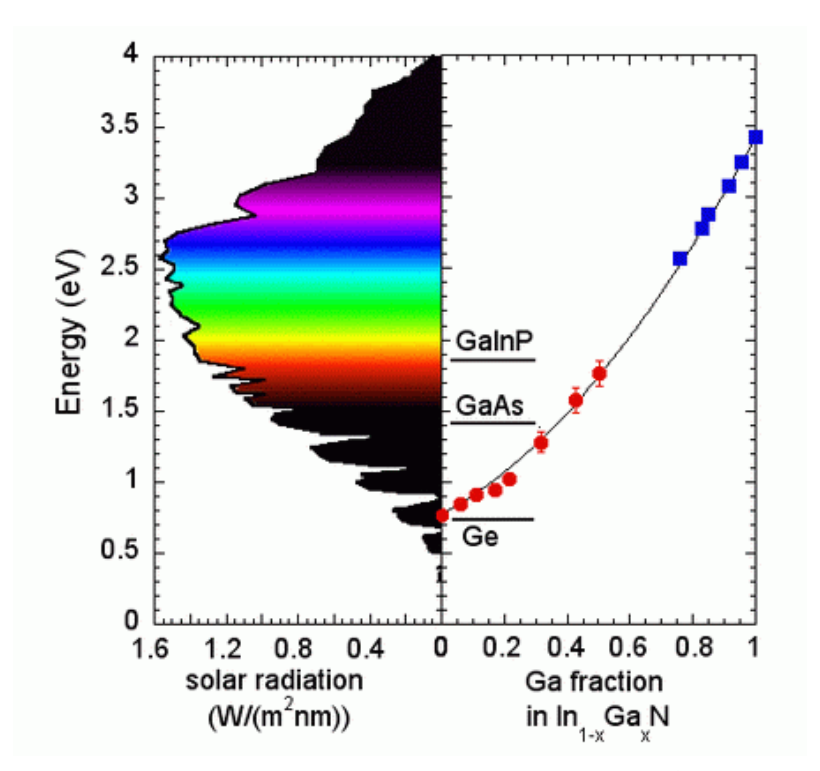
ผลการวิจัยเชิงคำนวณได้ทำนายคุณสมบัติในระบบสารผสมบางชนิด เช่น AlGaAs GaInP และ AlGaInP ที่ส่วนผสมต่าง ๆ พบว่านอกจากอัตราส่วนผสมแล้ว คุณสมบัติของสารขึ้นกับการ จัดเรียงตัวของโครงสร้างจุลภาคอย่างมากสอดคล้องกับสมมติฐานที่ตั้งไว้ การเรียงตัวในระดับจุลภาค เหนี่ยวนำให้เกิดการเปลี่ยนโครงสร้างของอิเล็กตรอนในสารมีผลกับคุณสมบัติเชิงไฟฟ้าและแสง ทำให้ พลังงานที่ใช้กระตุ้นอิเล็กตรอนต่ำกว่าค่าจากการประมาณแบบเชิงเส้นเป็นสาเหตุที่การประมาณแบบ เชิงเส้นใช้ไม่ได้ เช่น โครงสร้าง a) และ โครงสร้าง b) ดังรูป มีอัตราส่วนผสมเท่ากันแต่เรียงตัวต่างกัน ทั้งนี้พบว่าจะใช้การประมาณแบบเชิงเส้นได้ก็ต่อเมื่อการเรียงตัวของอะตอมในเนื้อสารเป็นแบบสุ่ม ผลลัพธ์นี้ช่วยให้นักวิจัยหรือผู้ผลิตสามารถประมาณช่วงของคุณสมบัติได้โดยไม่ต้องเตรียมสารตัวอย่าง ใดใด อีกทั้งระเบียบวิธีคำนวณและการวิเคราะห์ผลที่พัฒนาขึ้นสามารถใช้กับสารอื่นได้ทันทีโดยการ เปลี่ยนชนิดของอะตอมที่ใช้

งานวิจัยในระบบต้นแบบที่ได้สามารถประยุกต์ใช้กับการศึกษาแบบจำลองของสารผสมระบบ อื่น ๆ เปรียบเหมือนห้องทดลองเสมือน (Virtual Laboratory) ช่วยให้ผู้ที่สนใจทำการศึกษา ความสัมพันธ์ระหว่างคุณสมบัติของสารกับอัตราส่วนผสม และลักษณะการเรียงตัวของโครงสร้าง จุลภาคเพื่อหาแนวโน้มของคุณสมบัติที่จะได้ เป็นแนวทางก่อนเริ่มสังเคราะห์สารจริง และทราบถึง ข้อจำกัดของคุณสมบัติในสารนั้นเพื่อช่วยในการตัดสินใจเลือกสารที่จะใช้ผลิตชิ้นส่วนอุปกรณ์ ไม่ต้อง ลองผิดลองถูกช่วยให้ประหยัดทรัพยากรและเวลาในการสังเคราะห์สาร ช่วยลดต้นทุนชิ้นส่วนของ อุปกรณ์ที่ใช้ในด้านพลังงานทดแทน การส่งและเก็บข้อมูลด้วยแสง และเทคโนโลยีเลเซอร์ ทำให้เกิด การพัฒนาสารใหม่ ๆ ช่วยให้เข้าใจคุณสมบัติของวัสดุที่ได้ว่าสอดคล้องกับโครงสร้างอย่างไรต้อง ปรับเปลี่ยนกระบวนการสังเคราะห์อย่างไร

ระเบียบวิธีคำนวณและการวิเคราะห์ผลเชิงทฤษฎีเพื่อทำความเข้าใจและทำนายคุณสมบัติ ของสารมีส่วนช่วยในด้านการวิจัยและพัฒนาโดยตรงในอุตสาหกรรมวัสดุสารกึ่งตัวนำ ซึ่งใช้อย่าง แพร่หลายในด้านอิเล็กทรอนิกส์ พลังงานทดแทน และวัสดุเปล่งแสง สิ่งสำคัญประการหนึ่งคือสารกึ่ง ตัวนำมีคุณสมบัติพิเศษเพราะค่าช่องว่างแถบพลังงาน (Bandgap) หรือพลังงานที่ต้องใช้กระตุ้น อิเล็กตรอนให้เปลี่ยนระดับชั้นพลังงานไปสถานะนำไฟฟ้าสอดคล้องคลื่นแม่เหล็กไฟฟ้าในช่วงแสงที่

มองเห็นได้ พลังงานกับความยาวคลื่นแม่เหล็กไฟฟ้าสัมพันธ์ตามสมการ $E[eV] = 1240/\lambda [nm]$ มี พลังงานในหน่วยศักย์อิเล็กตรอน (eV) และความยาวคลื่นในหน่วยนาโนเมตร (nm) การควบคุมค่า แถบพลังงานโดยปรับส่วนผสมหรือการจัดเรียงตัวของสารมีผลกับสีของแสงในกระบวนการดูดกลืน หรือปลดปล่อยแสงของสารกึ่งตัวนำ

ตัวอย่างเช่น ความท้าทายในการพัฒนาประสิทธิภาพของเซลล์สุริยะ แสงอาทิตย์ ประกอบด้วยแสงสีต่าง ๆ เป็นแถบสายรุ้งโดยแต่ละสีมีความเข้มต่างกันดังรูป ถ้าใช้สารที่ดูดกลืนแสง เพียงบางค่าพลังงานก็เป็นการใช้แสงอาทิตย์ไม่ครบย่าน ดังนั้นเซลล์สุริยะที่ทำจากขั้นของสารผสม หลาย ๆ ชนิดที่มีการกระจายค่าพลังงานตั้งแต่รังสีใต้แดง (Infrared) จนถึงรังสีเหนือม่วง (Ultraviolet) เพื่อดูดกลืนแสงทุกสีให้ครบย่านจะเพิ่มประสิทธิภาพการใช้พลังงานอย่างมาก การ เข้าใจคุณสมบัติและข้อจำกัดของสารกับอัตราส่วนผสมเชิงทฤษฎีจึงจำเป็นอย่างยิ่งในการพัฒนา อุปกรณ์ ลดการสิ้นเปลืองทรัพยากรในการผลิต และเป็นเทคโนโลยีเพื่อสิ่งแวดล้อม (Green technology)



รูปภาพจาก http://www.lbl.gov/Science-Articles/Archive/MSD-full-spectrum-solarcell.html

Sirichok Jungthawan*, Kwiseon Kim, and Sukit Limpijumnong, The effects of unit cell size on the bandgap range in the direct enumeration study of $Al_xGa_yIn_{1-x-y}P$ alloys, Computational Materials Science 49, S114 (2010). JIF=1.522

Electronic structures of graphene/boron nitride sheet superlattices

Sirichok Jungthawan (莊俊強)^{1,2,3,*}, Sukit Limpijumnong^{1,2}, and Jer-Lai Kuo (郭哲來)^{3,†}

¹School of Physics, Institute of Science, Suranaree University of Technology and

Synchrotron Light Research Institute, Nakhon Ratchasima 30000, Thailand

²Thailand Center of Excellence in Physics (ThEP), Commission on Higher Education,

Ministry of Education, Bangkok 10400, Thailand

³Institute of Atomic and Molecular Sciences, Academia Sinica, Taipei 10617, Taiwan

Abstract

Structural stability of monolayer BC₂N is systematically investigated by means of

first-principles calculations with exhaustive enumeration of alloy configurations. The

energetically favorable configurations have a strong preference of large domain of BN and

graphene to form striped ordering with alternating domain of BN and graphene ribbons.

Properties of two edge structures (armchair or zigzag) are focused as they provide an

informative trend of the electronic properties related to edge modification and inversion

symmetry. We found that while formation energy monotonously decreases with increasing

size of domains, their electronic structure reveals special properties sensitive to the detailed

arrangement. The structures without inversion symmetry always have nonzero bandgap, in

which zigzag types show monotonic decrease and armchair ones exhibit triple periodicity

feature. But rearranging at the domain edges of BN and graphene, some structures can have

inversion symmetry and inversion symmetry introduces zero bandgap in zigzag type but not

in armchair type. Detailed analysis on the electric charge distributions shows that the

electronic properties of the monolayer BC₂N compounds strongly depend on the edge and

the size of domains.

*Corresponding author: sirichok@sut.ac.th, †E-mail address: jlkuo@pub.iams.sinica.edu.tw

1 of 25

I. INTRODUCTION

Once introduced, graphene [1-6], a single layer of graphite, holds a high hope for new generation electronic devices [1, 3] and hydrogen storage [7, 8]. In the last decade, graphene has been extensively studied because of its astonishing properties that are mostly attributed to quantum phenomena from 2D confinement effects [1, 5, 6]. In perfect graphene, each carbon atom forms σ -bonds with its three neighbors (sp^2 hybridization). The electronic states near the Fermi energy are the π and π^* bands derived from the weakly interacting p_z orbitals. The π and π^* states degenerated at the K point of graphene (hexagonal) Brillouin Zone, making graphene a zero-gap semi-metal. To utilize graphene as a semiconductor, several approaches to lift the degeneracy and open up graphene's gap have been introduced. They can be grouped into two categories according to Peng and Ahuja [9]: i) by confining or reducing the dimension [10-12] of graphene and ii) by placing graphene on a substrate that can break the equivalence of graphene sublattices A and B [9, 13].

In this work, a different approach to open up and control the graphene bandgap is proposed and computationally illustrated. We find that a bandgap and electronic structures of a superlattice (SL) structure between graphene and boron nitride (BN) sheet are vastly varied depending on the detailed superlattice structures. In semiconductors, many SL systems such as GaAs/AlAs and Si/SiO₂ SLs (to name a few) of various dimensions and orientations have been studied both computationally and experimentally. Graphene superlattices have been previously studied by Park *et al.* [14-16]. Electronic properties of SLs are shown to be sensitive to the detailed SL structures and orientations. Here, we will show that the electronic properties of graphene/BN SL are even more sensitive to the SL structures and orientation; opening up an opportunity to engineer graphene's electronic properties.

Boron nitride (BN) can form in numerous structures in analogous to carbon (C). The main reason is because boron and nitrogen can have different hybridization of chemical

bonding (e.g., sp^2 and sp^3). Bulk BN can form in *hexagonal*-BN (*h*-BN) [17] and *cubic*-BN (*c*-BN) [18] structures which are analogous to graphite and diamond in carbon system. Various forms of BN nanostructures have also been reported [19-23]. A monolayer BN (1-BN) is formed by sp^2 bonds and is structurally similar to graphene with the B-N bond only 1.7% larger than C-C bond in graphene. The electronic properties of 1-BN, on the other hand, are different from those of graphene. For instance, 1-BN is an insulator with a direct bandgap at the *K* point. These make 1-BN a suitable material to form superlattice with graphene. [Strictly speaking, 1-BN has a space group $P\overline{6}m2$ which is differed from graphene (P6/mmm) due to the lacking of inversion symmetry (the difference between the two sublattices in the unit cell). This symmetry lacking is actually responsible for the difference in the degeneracy at the *K* point of the BZ [24, 25].]

SLs are actually special cases of the alloy systems between BN and C. From an alloy viewpoint, monolayer BC_xN (1-BC_xN) alloys have been studied theoretically by various groups [24, 26-28]. Previous reports showed that the structural stability of 1-BC_xN depends strongly on the bond energies. It was shown that B-N and C-C are highly favored while the B-B, N-N, B-C, and C-N bonds have higher energies [24, 26-29]. These influence the structural arrangements, i.e., pattern and domain shape. The energetically favorable structures tend to maximize B-N and C-C bonds [24, 26, 27]. As a result, the system tends to have phase segregation into large BN and C domains [29, 30]. The similar behaviors have been observed for the cases of BC_xN nanotubes and heterostructures [20, 21]. Monte Carlo study also shown [29] that 1-BC_xN have strong preference to form B-N and C-C bonds; suggesting the phase separation into 1-BN and graphene. Despite a tendency to form phase separation, at sufficient temperature, lattice vibration can enhance the solubility and a solid solution can be expected [29]. Experimentally, some stable BC₂N have been successfully synthesized [31, 32].

On the theoretical side, some atomic arrangements of monolayer BC₂N (1-BC₂N) has also been studied [24, 26-28]. Liu et al. [24] proposed a model that B, C, N-atoms arrange into alternating stripe of B-N and C-C molecular chains (a simple SL case). Nozaki and Itoh [27], and Azevedo et al. [26, 28], studied the monolayer arrangements using a large unit cell and proposed the island-like models of BN domain in C and vice versa. Recently, a 1-BC_xN was experimentally studied [33] and the BN domains in graphene have been observed consistent with theoretical predictions. Depending on the alloy composition and growth condition, the phase separation can give either the BN domain in C or vice versa. In some special compositions such as BC₂N, the SL structures (striped pattern) can be more energetically favorable over the island patterns [27]. This is consistent with our first principles enumeration study (details will be published elsewhere) which found the SLs (striped patterns) to be low energy configurations for 1-BC₂N. In various experimental and natural systems, striped patterns frequently arise as energetically favored ground states where the universality of striped morphologies have been discussed by Edlund and Jacobi [34]. In this work, we will focus our attentions on the electronic properties of graphene/1-BN SLs with different widths and orientations. As a starting point, we limited our study to only the SLs with equal amount of graphene and BN (i.e. 1-BC₂N).

II. METHOD

In Fig. 1, a few supercells used for studying graphene/1-BN in the SL configurations along with their corresponding BZ are shown. Based on the symmetry, two most relevant orientations of the SLs, i.e. zigzag (Z) or armchair (A) molecular chains, are studied. The SL width is defined by the number of chains (N) in a layer. We refer to a zigzag and armchair SL configurations with N-alternating chains as NZ and NA, respectively. Because of the difference between B and N atom, on a closer inspection, one can see that a supercell containing a single strip each of C and BN does not give a SL structure with inversion

symmetry. To generate a SL with an inversion symmetry, a supercell size has to be doubled. For examples, 2Zi, which refers to a SL containing two zigzag alternating chains with inversion symmetry, is doubled of 2Z. In this work, we focus our attentions on ordinary oriented SLs (i.e., NZ and NA) and their inversion symmetry counterparts (i.e., NZi and NAi) with $1 \le N \le 6$.

The calculations were performed based on the density functional theory [35] within local (spin) density approximation (LDA) [36] and the projector augmented wave (PAW) potentials [37, 38] as implemented in the VASP code [39-41]. The cutoff energy of the plane wave expansion is 600 eV. The Γ -centered Monkhorst-Pack scheme with the k-mesh varying based on the dimension of the BZ is used for BZ integration, for instance, $36\times20\times1$ for 1Z unit cell. The convergence for electronic step is 0.1 meV. The vacuum spacing of 15 Å is used to prevent interactions between the adjacent layers. Structural relaxation is performed without symmetric constraint until the force on each ion is less than 0.01 eV/Å. For each configuration, cell shape optimizations (a and b/a ratio) are performed. The formation energy of each 1-BC₂N configuration is referenced to the segregated phases (1-BN and graphene) which is defined as

$$E_{
m form}~X~=E_{
m total}~X~-~E_{
m BN}+E_{
m graphene}$$
 ,

where $E_{\rm total}~X~$ is total energy per formula (BC₂N) of configuration X, $E_{\rm BN}$ and $E_{\rm graphene}$ are the total energy per pair of 1-BN and graphene; referenced to the energy of isolated atoms (the numerical values are shown in Table 1).

III. RESULTS AND DISCUSSION

A. Structural stability

Our enumeration study of a large number of 1-BC_2N configurations (details will be published elsewhere) shows that the energetically favorable configurations have a strong

preference to form phase separated BN and graphene, i.e. minimizing B-C and C-N bonds while maximizing B-N and C-C bonds. This can be done by forming SLs (stripe patterns). In this work, we focus our attentions on two most relevant types of SLs, i.e. armchair and zigzag types as explained in the previous section. Note that more complicated SLs (along other directions) can be formed with the mixing of the armchair and zigzag molecular chains but are not covered in this work.

The formation energy per chemical formula and bandgap of SLs with different widths are shown in Fig. 2. In all cases, the formation energy monotonously decreases with increasing N. This is not surprising because the wider SL allows more preferred bonds to form and reduce the fraction of atoms on the boundary between BN and graphene. For the armchair SLs, the energy decreases from 0.90 eV for 1A to 0.18 eV for 6A and slightly decreases further for larger N. If we compare between the SLs with armchair and zigzag edges, it is found that NAs are slightly more energetically favorable than NZs. The relative stability between NZ and NA is 0.04 eV for N = 1 and increases to 0.08 eV at large N. Armchair SLs provide more degree of relaxation than zigzag SLs at the domain edges. For larger N, the higher energy of the zigzag SL over the armchair SL (with the same N) can be attributed to the accumulation of charge at the edges. Because the zigzag SLs have one type of edges with all B-C bonds and another type of edges with all C-N bonds, the edges with the B-C bonds are less electronegative than the edges with C-N bonds. As a result, the edges with C-N bonds are more negative while the edges with B-C bonds are more positive. This leads to the charge transfers and formation of line charge at the edges. The formations of line charges cost energy (while the interaction between the line charges with opposite sign reduces it). On the other hand, all edges of armchair SLs composed of an equal number of B-C and C-N bonds. As a result, no line charges are formed; making the armchair SLs more energetically favorable. The charge accumulated on the edges of the zigzag SLs will be clearly seen when we discuss about the electron charge density plots near the Fermi energy. In additional to the energetic stability, as will be seen next, the charge accumulation on the edges greatly affects graphene electronic properties because it introduces electric fields across the graphene stripe.

The ordered SLs with inversion symmetry (NZi and NAi) have higher energy than their counterparts without the inversion symmetry (NZ and NA). For example, the difference between 1Zi and 1Z is 0.28 eV; 1Ai and 1A is 0.13 eV. Note that the energy difference between the SLs with inversion symmetry and their counterparts decreases as N increases and becomes negligibly small at $N > \approx 6$, as can be seen in Fig. 2. The larger energy difference for the zigzag SLs can be attributed to the Coulomb interaction between the edges. For the SLs without inversion symmetry, the B-N bonds in all BN stripes are pointing in the same direction. Therefore, the left edge and right edge of the graphene stripe are not the same (in Fig. 3a, the left edge is the edge with N-C bonds whereas the right edge is the edge with C-B bonds); leading to alternated positive/negative line charges. These line charges create an electric field across the graphene stripes; affecting the bandgap as will be explained in the next section. For the SLs with inversion symmetry, the B-N bonds in two BN stripes sandwiching the graphene stripe are pointing in opposite directions to maintain the inversion symmetry. As a result, the left and right edges of any graphene stripe are equivalent, i.e. either the edges with B-C bonds or the edges with C-N bonds; leaving no electric field across the graphene stripe. When compare the ordering of the edges, we can see that the SLs without inversion symmetry have the ordering of line charges with period of +-, compare to ++-- in the SLs with inversion symmetry. Because the Coulomb attraction would gain energy when the opposite charges are placed next to each other and cost energy when same charge are placed next to each other, the SLs with inversion symmetry have higher energy than their counterparts. The line charges at the edges are separated apart by the stripes with the width proportional with *N*. This explains why the SLs with larger stripes have reduced energy differences.

For the *armchair* SLs, the energy differences between the non-inversion and inversion ordering are smaller than those of the zigzag SLs. This is because each armchair edge composed of an equal number of B and N atoms; leading to neutral charge. The energy differences (between the SLs with and without inversion symmetry) arise from the small differences in the distances of B-to-B, N-to-N, and B-to-N across the graphene stripe. The SLs with the inversion symmetry have slightly shorter B-to-B and N-to-N distances (and longer B-to-N distances) than their counterparts causing higher energy. Although the armchair edges have total neutral charge, the B and N atoms at the edges are containing opposite charge. The differences in the distances as well as the Coulomb interactions diminished quickly as the SL stripe gets wider (larger *N*).

The electronic properties of these SLs are discussed in section III-B and III-C.

B. Electronic structure of zigzag superlattices

The BZ of 1Z SL, is related to the fundamental graphene BZ (hexagonal) by the folding of the hexagonal BZ in a rectangular BZ of 1Z shown as a white filled region in the top panel of Fig. 1. The folding places the high symmetry points M' on Γ . The two K' and a K points of the graphene BZ are folded to the same point in 1Z BZ at 2/3 of the symmetry line between the Γ and X points. Asymmetric interaction between two K' and a K points slightly shifts the top of valence band maximum (VBM) and the bottom of conduction band minimum (CBM) away from the original K toward the X direction as can be seen in the band structures plot (Fig. 4).

As the stripe of the zigzag SL getting wider the bandgaps decrease, i.e., the bandgap monotonously decreases with increasing N. For N=1 the bandgap is the largest at 1.6 eV and gradually decreases down to almost zero at N=6, as shown in the right panel of Fig. 2. Note

that these bandgaps are direct DFT-LDA results and are expected to be too small due to the well-known DFT-LDA bandgap problems. The bandgap reduction as N increases can also be observed in the band structures plots in Fig. 4 (the top of VBM and the bottom of CBM get closer in the band structures of larger N SLs). The band structure plots show that states near the Fermi energy lie in the k-space region in the vicinity around the lines between K and X points. To examine the electronic states near the Fermi level, charge densities of the states near the Fermi energy are plotted. As a representative case, the charge densities of the states of 6Z SL near the Fermi level (indicated by orange arrows in Fig. 4) are shown in Fig. 3. The VBM and CBM states are found to be localized on the edges, as shown in Fig. 3(a) and (b), respectively. Because the VBM states are occupied and the CBM states are unoccupied, the electric potential is formed across the graphene stripe. The states near the VBM have the p_z π -bonding character and are highly localized on the C-B edges. On the other hand, the states near the CBM have the p_z π -antibonding (π^*) character and are highly localized on the N-C edges. The charge accumulation on the edges gives rise to the electric field across the graphene stripe leading to bandgap opening [42]. For graphene nanoribbons (GNRs), the bandgap opening also attributed to the electric field from the edges [43]. In GNRs, the electric potential at the edges is originated from the spin orientation. For the cases at hand, the electric potentials are created by the difference in the bonding chemical at the two edges around the graphene stripe (B-C and C-N bonds) [44]. The charge accumulation at the edges for SLs with different widths is very similar. Therefore, the wider SLs (large N) have smaller electric field across the graphene stripes, leading to smaller bandgap openings.

Unlike the zigzag SLs without inversion symmetry, the NZi SLs always have zero bandgap. They have linear dispersion crossing near the X point. Because of the inversion symmetry, each graphene stripe in NZi have the same bond type at both edges (i.e., either B-C or C-N). This results in no electric field across the graphene stripes. The band structures

of selected zigzag SLs with inversion symmetry are show in Fig. 4. The VBM and CBM are highlighted. The four states near the Fermi level, i.e., the highest two valence bands (VBM and VBM-1) and the lowest two conduction bands (CBM and CBM+1) are localized at the edges. The VBM and VBM-1 states have the p_z π -bonding character at the B-C edges whereas the CBM and CBM+1 states have the p_z π -antibonding (π^*) character at the C-N edges, as shown in Fig. 3(c) and (d), respectively. Because both edges of graphene stripes are equivalent, there is no electric field across the graphene stripe and no bandgap opening. When the number of zigzag chain is odd (N = odd), the edge termination is nonsymmetrical staggered. Along high symmetry XR line, the bonding and antibonding states are degenerated (1Zi and 3Zi in Fig. 4). When the number of graphene layer is even (N = even), the structures retain a single mirror symmetry plane (perpendicular to the plane of the sheet and containing the center line of graphene stripe). The edge termination is symmetric along the domain axis. As a result, the bonding and antibonding states become nondegenerated state along XR line (6Zi in Fig. 4). The pseudo bandgap (quadratic dispersion curves near crossing) decreases with increasing N and goes to zero (overlapped) when N > 3.

The electronic states attributed to B-C and C-N at the edges can be qualitatively understood within the tight-binding model. The Hamiltonian based on the nearest-neighbor tight-binding model is defined by

$$H = \sum_{i} \varepsilon_{i} a_{i}^{\dagger} a_{i} - \sum_{i,j} t_{ij} a_{i}^{\dagger} a_{j}, \tag{1}$$

where ε_i is the site energy atom at the site i, t_{ij} is the hopping integral between the site i and j, a_i^\dagger and a_i is the creation and annihilation operator of the π electron at the site i. The summation is taken over the first nearest-neighbor sites. In our case, we have three site-energy parameters defined as $\varepsilon_{\rm B}>0$, $\varepsilon_{\rm C}=0$, and $\varepsilon_{\rm N}<0$ and four hopping parameters

 $t_{\rm CC}$, $t_{\rm CB}$, $t_{\rm CN}$, and $t_{\rm BN}$ (all are positive). The site energies and all t parameters were adjusted to qualitatively investigate the supperlattice configurations.

Within tight-binding model, zigzag graphene nanoribbons (ZGNRs) are always metallic [45, 46] and zigzag boron nitride nanoribbons (ZBNRs) are wide-bandgap semiconductor. The electronic structure of zigzag SLs can be considered as metallic ZGNR electronic structures embedded in the gap of ZBNR as shown in Fig. 5 for zigzag SL with one molecular chain (ZGNR/ZBNR). The transfer energy between ZGNR and ZBNR at the edge ($t_{\rm CB}$ and $t_{\rm CN}$) lifts the degeneracy of the ZGNR edge-states at X. The B-C/C-N state (Fig. 5) is moved down/up and becomes VBM/CBM for both NZ and NZi SLs (Fig. 5) as verified by electron charge distribution in Fig. 3. For NZ, the $t_{\rm CB}$ and $t_{\rm CN}$ lift the degeneracy of the ZGNR edge-states and open up bandgap. For NZi, the inversion symmetry allows the crossing between B-C and C-N states causing zero bandgap.

C. Electronic structure of armchair superlattices

For the smallest armchair SLs (1A), the unit cell is twice larger than that of 1Z. Therefore, the BZ of 1A is half of 1Z BZ and is related to it by folding which place the X point of 1Z BZ at Γ . The BZ of 1A is shown as white filled region in the bottom panel of Fig. 1. The original K' and K points are located on the ΓX line at 2/3 toward X. For armchair SLs (NA), the location that the original K points fold into depends on N. For instance, the two K points are folded onto Γ when N is a multiple of 3. When N is not a multiple of 3, the K points get folded closer to Γ as N increases (and the direct bandgap is expected to move closer to Γ). Unlike the zigzag ordered SLs, the states near the Fermi energy are not localized on the edges.

The bandgaps of NA SLs are shown in the right panel of Fig. 2. These NA SLs always have bandgap opening. Overall, the bandgap appears to decrease as N increases.

However, the trend of the bandgap versus N has an interesting triple periodicity pattern. The triple periodicity pattern has also been observed in GNRs [43, 46] which depends on the number of dimer lines, N_a . However, in our case, N is the number of chains. In armchair graphene nanoribbons (AGNRs), the bandgap has been attributed to the abrupt changing of the bond lengths of the edge atoms which induce more hopping integral between π -orbitals [43]. The increase of the hopping integrals between C atoms at the edges is responsible for the correction to the zeroth-order bandgaps categorized into three different groups. For NA SLs, the triple periodicity in bandgaps is related to the BZ folding. When N is a multiple of 3, the original K points are folded onto Γ allowing the strong interaction between VBM and VBM-1 as well as CBM and CBM+1.

For the armchair SLs with the inversion symmetry (NAi), the bandgaps are smaller than their counterparts as shown in the right panel of Fig. 2. The lowest (highest) two conduction (valence) band states are degenerated state when $N \ge 3$ as shown for the case of 3Ai in Fig. 6. Along the high symmetry XR line, the states are degenerated. In the armchair SLs, the two hexagonal sublattices lie on the same line of the molecular chains. For the armchair SLs without inversion symmetry (NA), the B-N bonds at the edges align in the same direction introducing the dipoles with the same direction on both edges. On the other hand, the armchair SLs with inversion symmetry (NAi), the B-N bonds at the two edges sandwiching the graphene stripe align on the opposite direction. As a representative case, by examining the charge density distribution of 6A and 6Ai SLs (Fig. 7), we can see that the direction of edge dipoles affects the hybridization of states in the whole graphene stripe. For 6A, the dipoles at the edges induced the splitting of the π -bond hybridization in the graphene stripe into two groups; the bonds that are parallel to the dipole direction and that are vertical to them. For 6Ai, because the dipoles at both edges are aligned in opposite directions, the π -bond in the graphene stripe hybridized in the direction accommodating the dipoles of both

edges. Unlike the zigzag SLs where the CBM and VBM states are localized on the edges, the CBM and VBM states of the armchair SLs are spread throughout the graphene stripe. The charge distribution of VBM and VBM-1 are shown in Fig. 7(a)-(b) for 6A and Fig. 7(c)-(d) for 6Ai, respectively. Note that, the charge distribution of CBM is also spread in the graphene domain and not shown here. For 6A [Fig. 7(a), (b)], although the separation between VBM and VBM-1 is small, the two states show the non-degenerated signature (the π -bond hybridizations that are orthogonal to each other). For 6Ai [Fig. 6(c), (d)], VBM and VBM-1 are degenerated and the charge density of both states is similar. The opposite polarization at the C edges decrease bandgap of armchair ordered structures. All *N*Ai SLs also have non zero bandgaps, except 1Ai where there is only a single molecular chain defining the graphene stripe. The states near the Fermi energy are, therefore, dispersed in both BN and graphene stripes as shown in Fig. 7(e); resulting in zero bandgap.

Within tight-binding model, armchair AGNRs are either metallic ($N_a=3p+2$ where p is integer) or semiconducting ($N_a=3p$ and $N_a=3p+1$), depending on N_a [43, 46], and armchair boron nitride nanoribbons (ABNRs) are wide-bandgap semiconductor. The NA and NAi SLs with N=1,4,7,... have the number of dimer lines in graphene domain equal to $N_a=2,8,14$, respectively, which correspond to metallic AGNR ($N_a=3p+2$). The other NA and NAi SLs with N=2,3,5,6,... are correspond to semiconducting AGNR. The electronic structure of these SLs can be considered as the electronic structure of AGNR, either metallic or semiconducting, in ABNR bandgap. The transfer energy at the edge (t_{CB} and t_{CN}) affects to the bonding of the edge atoms thus opens up bandgap. Although the inversion symmetry allows the crossing along ΓX , the transfer energy at the edge opens up bandgap therefore the effect from inversion symmetry can reduce, but not enough to close, the gap. As a result, SL with inversion symmetry has lower bandgap compared with the same

size of SL without this symmetry. For 1Ai which is metallic, the transfer energy at the edge causes an even redistribution of charge on graphene domain as shown in Fig. 7(e) such that the splitting of AGNR metallic state is small thus the crossing by the inversion symmetry is observed.

IV. SUMMARY

The atomic arrangements of monolayer BC₂N were studied by enumerating unique arrangements and avoiding disfavored B-B and N-N neighboring, within all distinct 8-atoms cell. The energetically favorable configurations have a strong preference of large domain of BN and graphene reducing disfavored bonding (B-C and C-N) at the domain edge over favored bonding (B-N and C-C) in the domains. The energetically favorable configurations suggest striped ordering with alternating B-N and C-C molecular chains in BC₂N. The formation energy decreases as the number of chain increases. The armchair molecular chains are more stable in energy than the zigzag molecular chains. The structural stability and electronic properties depend strongly on the chemical bonding at the domain edges. The structures without inversion symmetry always have nonzero bandgap. The armchair and zigzag ordering have bandgaps which decrease as the number of chains increase. The ordered configurations with inversion symmetry always have smaller bandgap than ordinary ordered configurations for armchair ordering. The bandgaps are always zero for zigzag ordering with inversion symmetry. In conclusion, the configurations without inversion symmetry always have non-zero bandgap and the configurations with inversion symmetry may or may not have zero bandgap as proposed by Liu et al. [24]. The properties of the monolayer BC₂N compounds strongly depend on the edge and the size of domains.

Acknowledgments

We acknowledge fruitful discussions with Prof. Mei-Yin Chou. This work is financially supported by Thailand Research Fund (Grant No. MRG5280235), Academia Sinica, the National Science Council of Taiwan (Grant No. NSC98-2113-M-001-029-MY3), and National Center for Theoretical Sciences (South), Taiwan.

FIG. 1 (Color online) The zigzag and armchair superlattice with one and two alternating molecular chains. The blue, red, and black colors represent B, N, and C. The 1st BZ of fundamental ordered structures (1Z and 1A) is shown together with the primitive (unfolded) hexagonal BZ. The red line shows the 1st BZ of higher ordered structures with $2 \le N \le 6$ (see text). The high-symmetry points X, Y, and R of ordered structures indicate zone-edge in \hat{x} , \hat{y} , and corner point respectively. The inversion center is guided by star symbol.

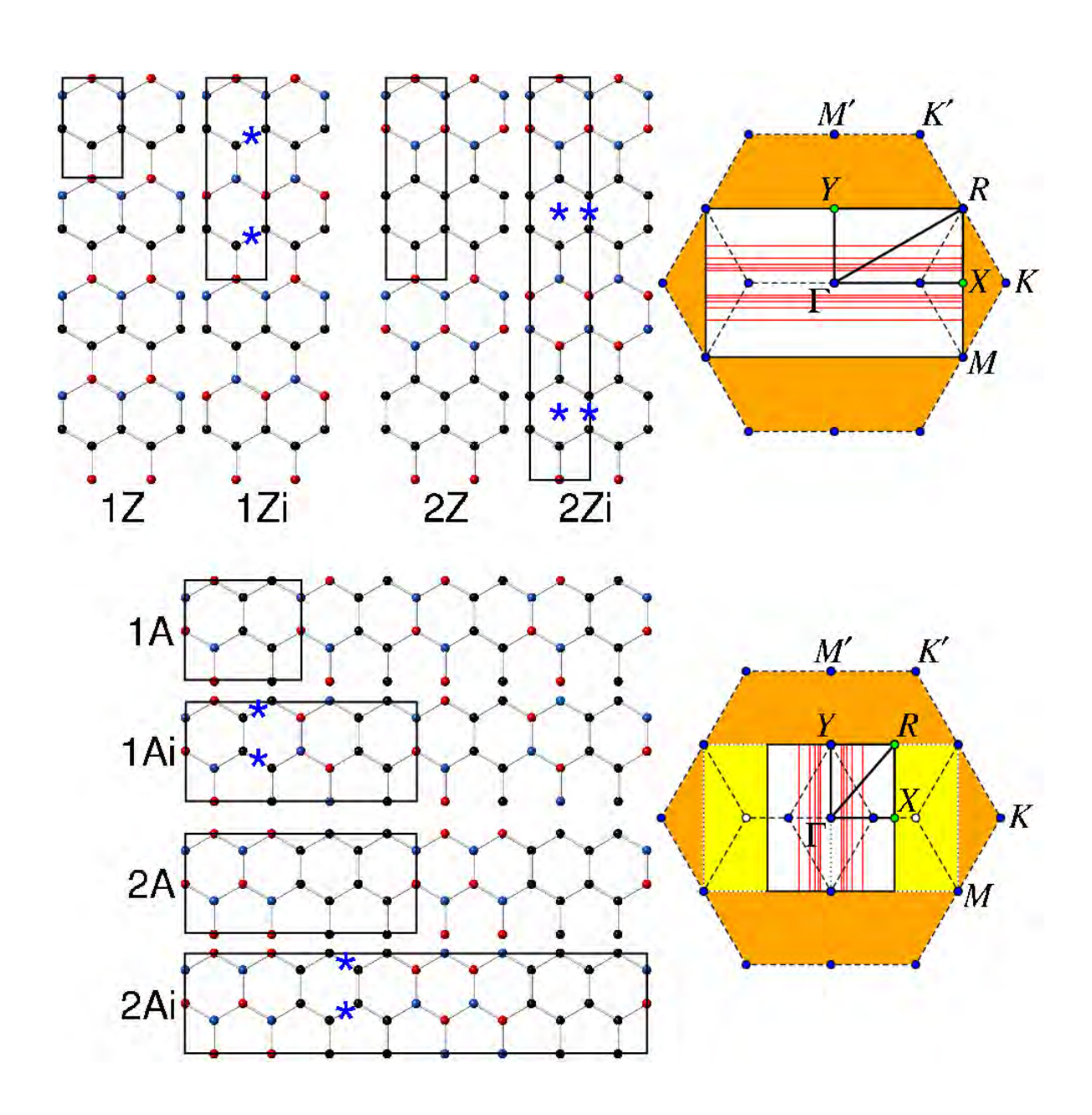


FIG. 2 (Color online) The formation energy (left panel) and calculated LDA bandgap (right panel) of ordered structures with different N. The blue and red solid line represents ordinary zigzag and armchair superlattice. The zigzag and armchair superlattice with inversion symmetry are represented by blue and red dashed line.

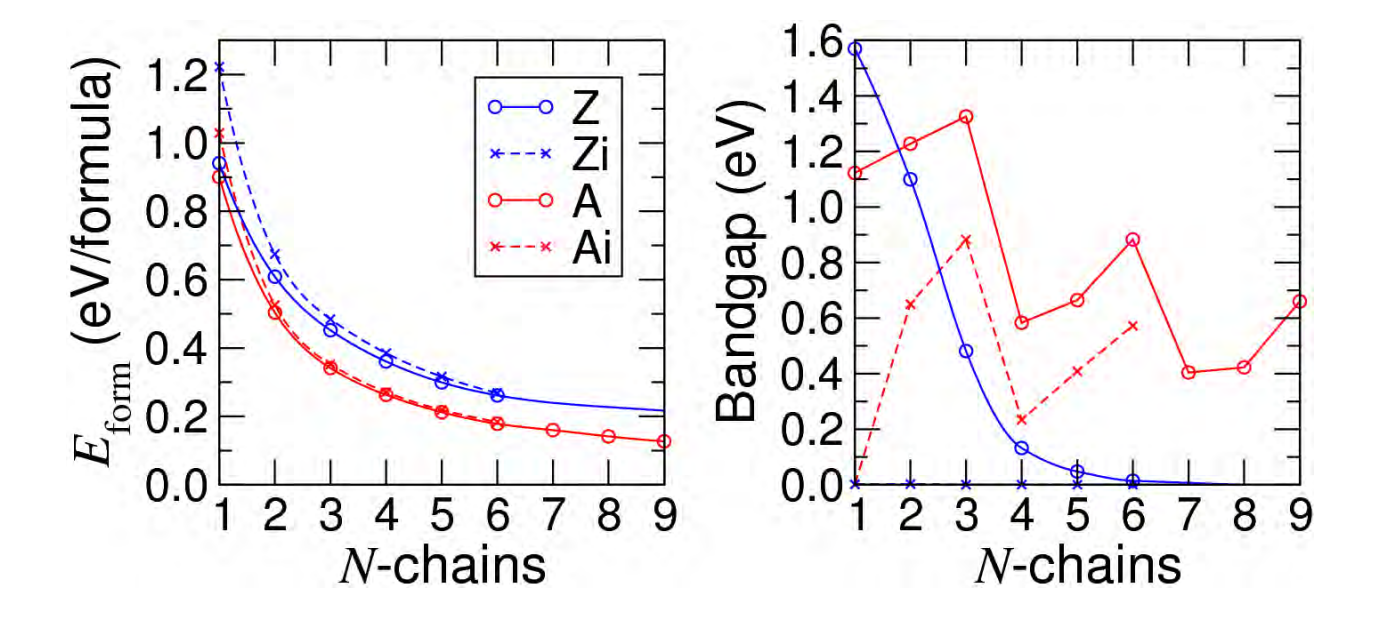


FIG. 3 (Color online) The electron charge density distribution near X point (indicated by orange arrows in Fig. 4) associated with the top of valence band of 6Z (a), the bottom of conduction band of 6Z (b), the sum of the highest two valence bands of 6Zi (c), and the sum of the lowest two conduction bands of 6Zi (d). The blue, red, and black colors represent B, N, and C.

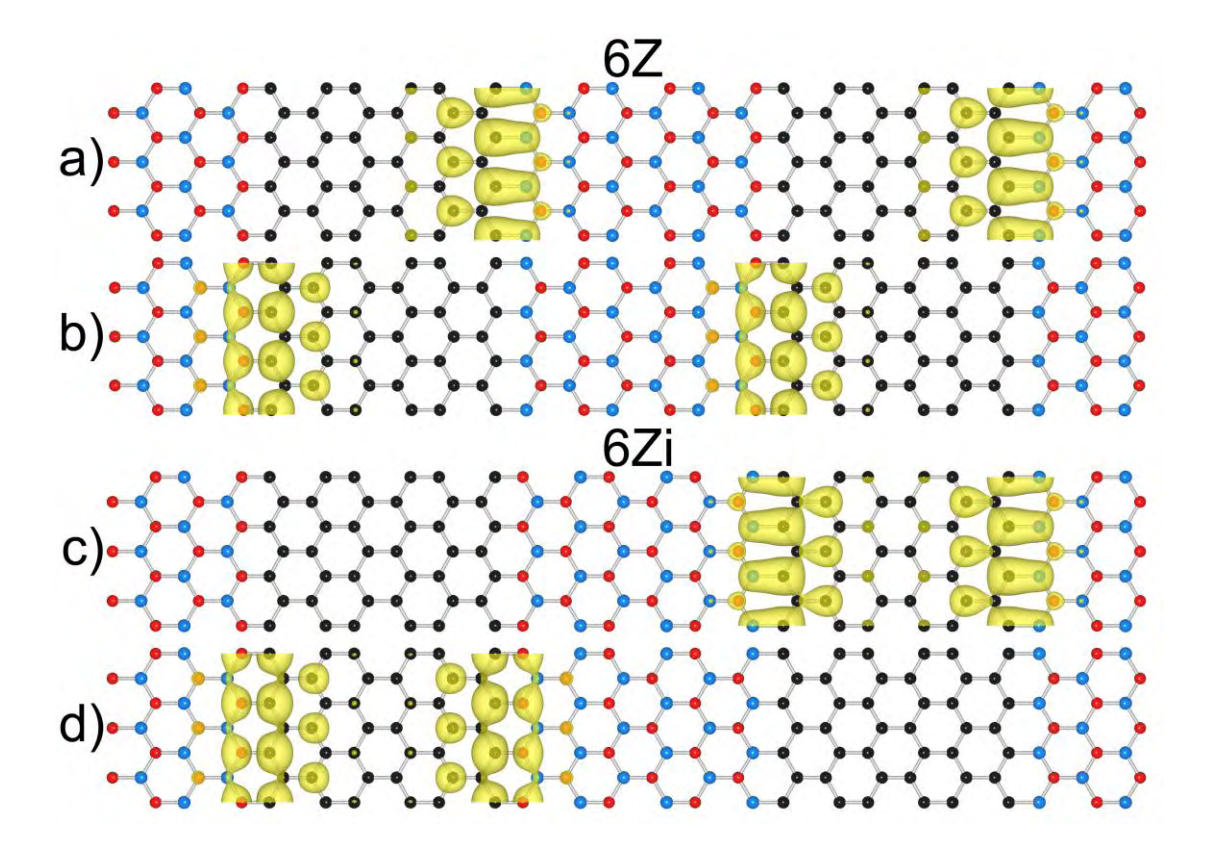


FIG. 4 (Color online) The calculated band structures of the zigzag (1Z, 2Z, 6Z, 1Zi, 3Zi, and 6Zi) ordered structures plotted along the symmetry points in the BZ as described in Fig. 1. The orange arrows indicate the point where electron charge density distributions are obtained in Fig. 3.

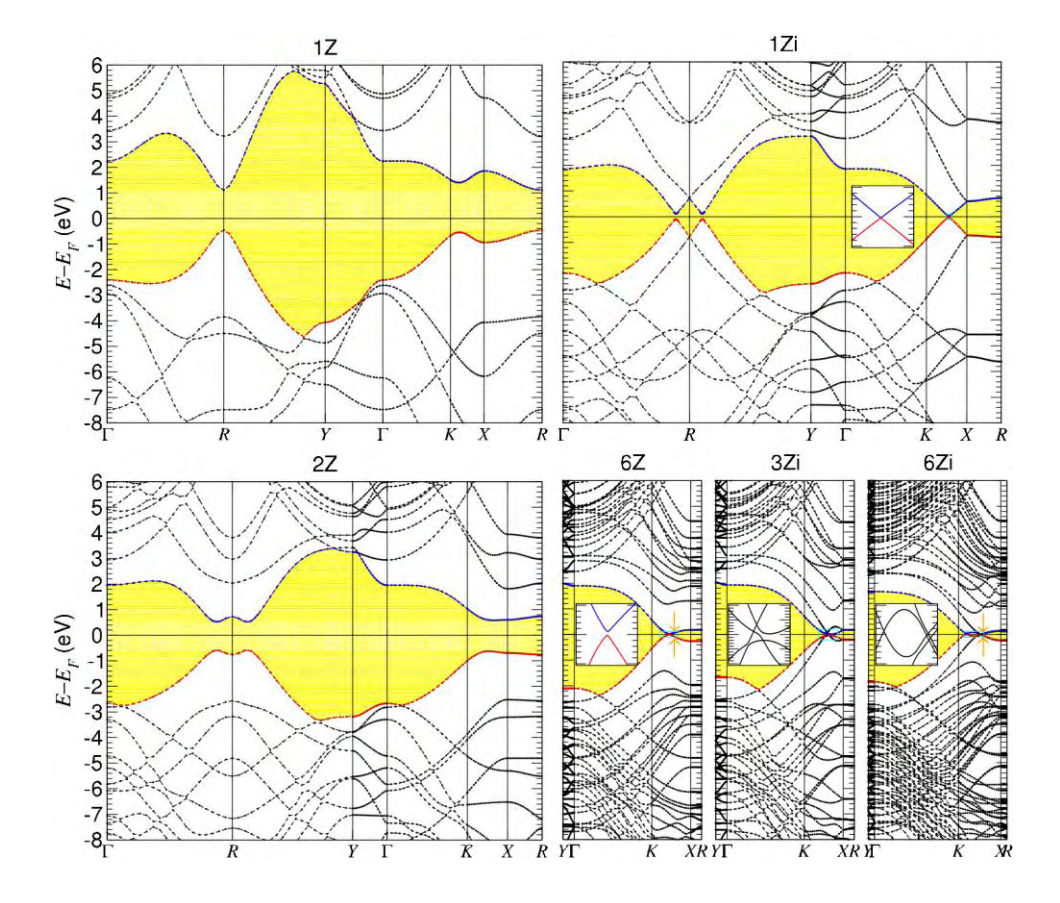


FIG. 5 The band structure plots, along Y- Γ (dashed line) -X direction, of zigzag and armchair superlattices with one alternating molecular chain from tight binding method. The non-interacting GNR/BNR SLs with zigzag (ZGNR/ZBNR) and armchair (AGNR/ABNR) ordering are shown for reference.

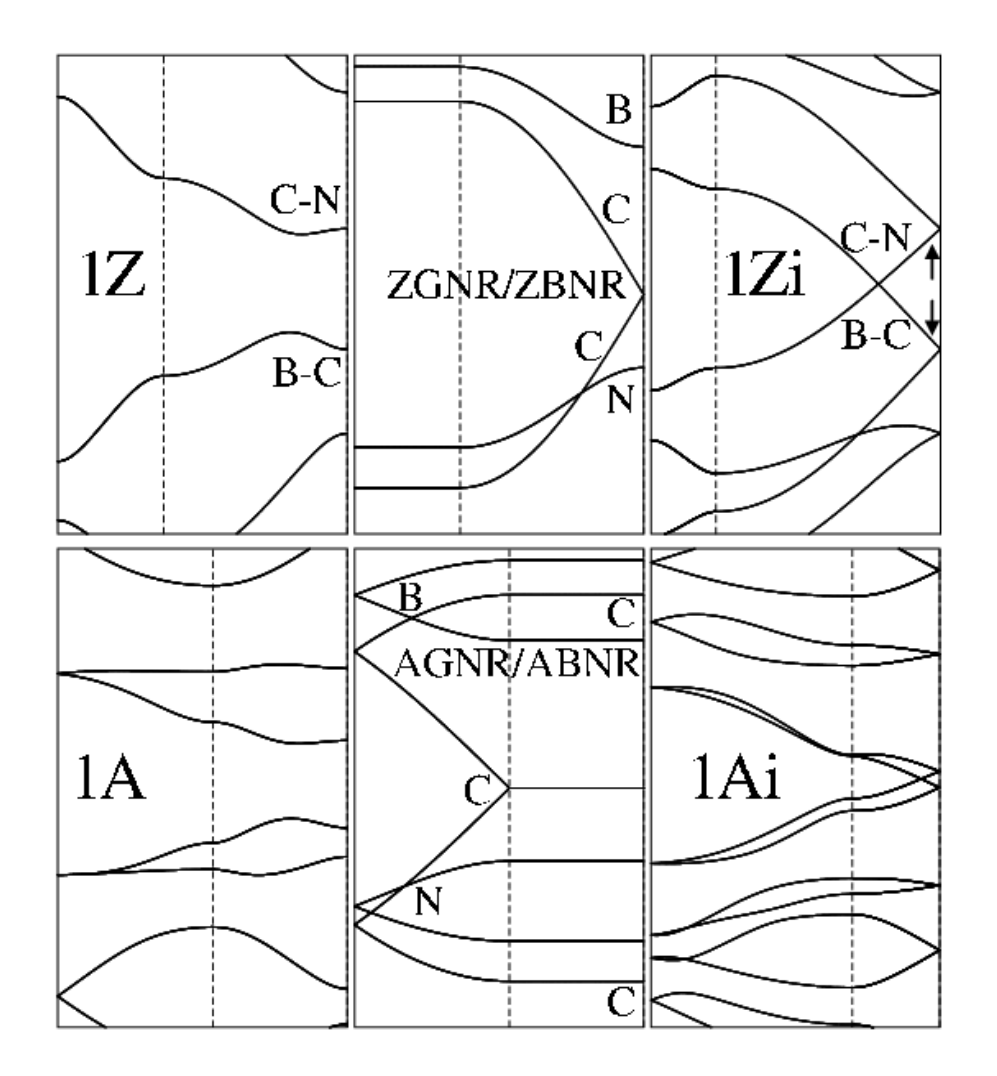


FIG. 6 (Color online) The calculated band structures of the armchair (1A, 2A, 4A, 5A, 6A, 1Ai, 2Ai, and 3Ai) ordered structures plotted along the symmetry points in the BZ as described in Fig. 1.

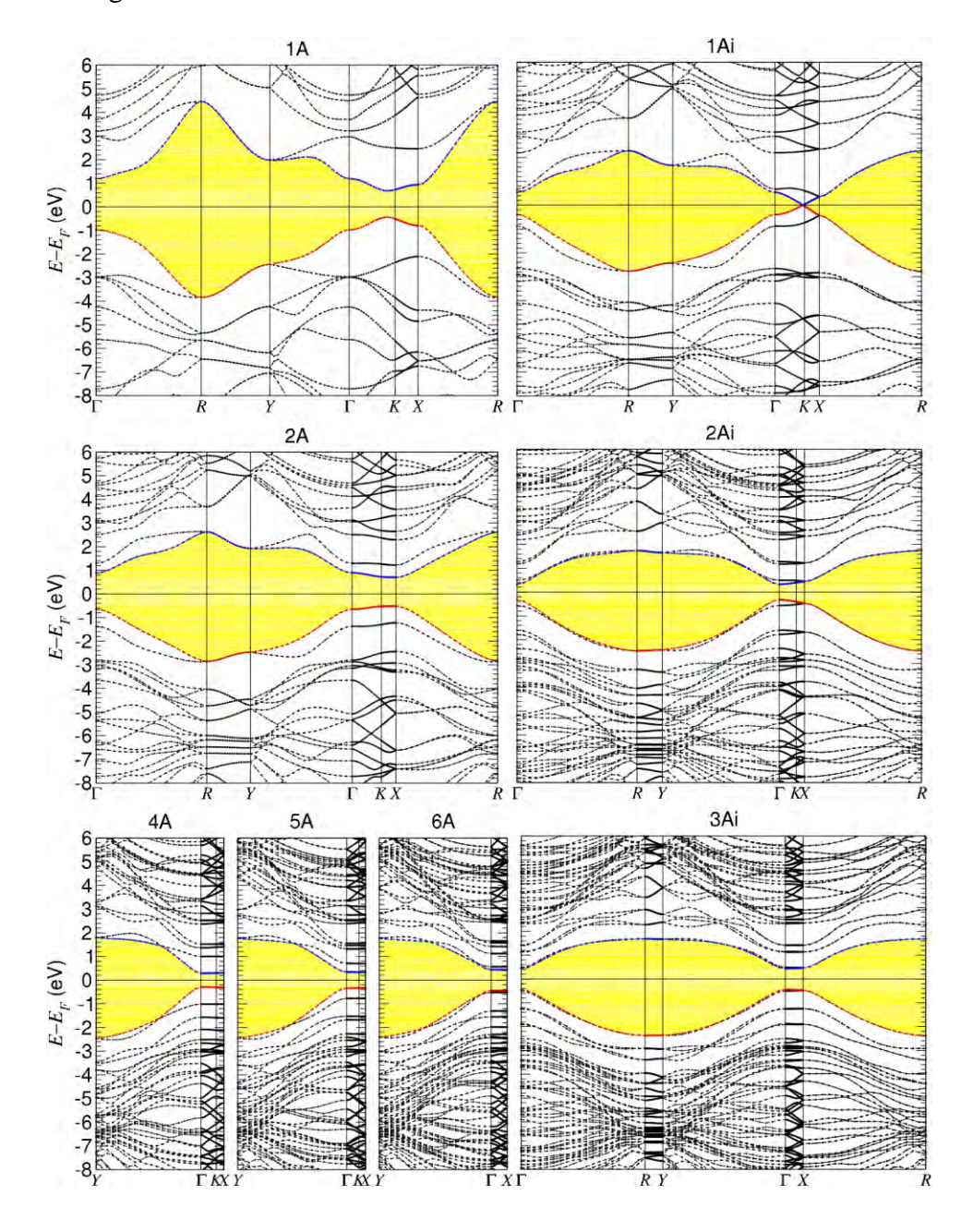


FIG. 7 (Color online) The electron charge density distribution associated with; the highest two valence bands (VBM and VBM-1 respectively) at the Γ point of 6A [(a) and (b)], 6Ai [(c) and (d)], and the top of VBM near the K point (Fig. 6) of 1Ai (e). The blue, red, and black colors represent B, N, and C.

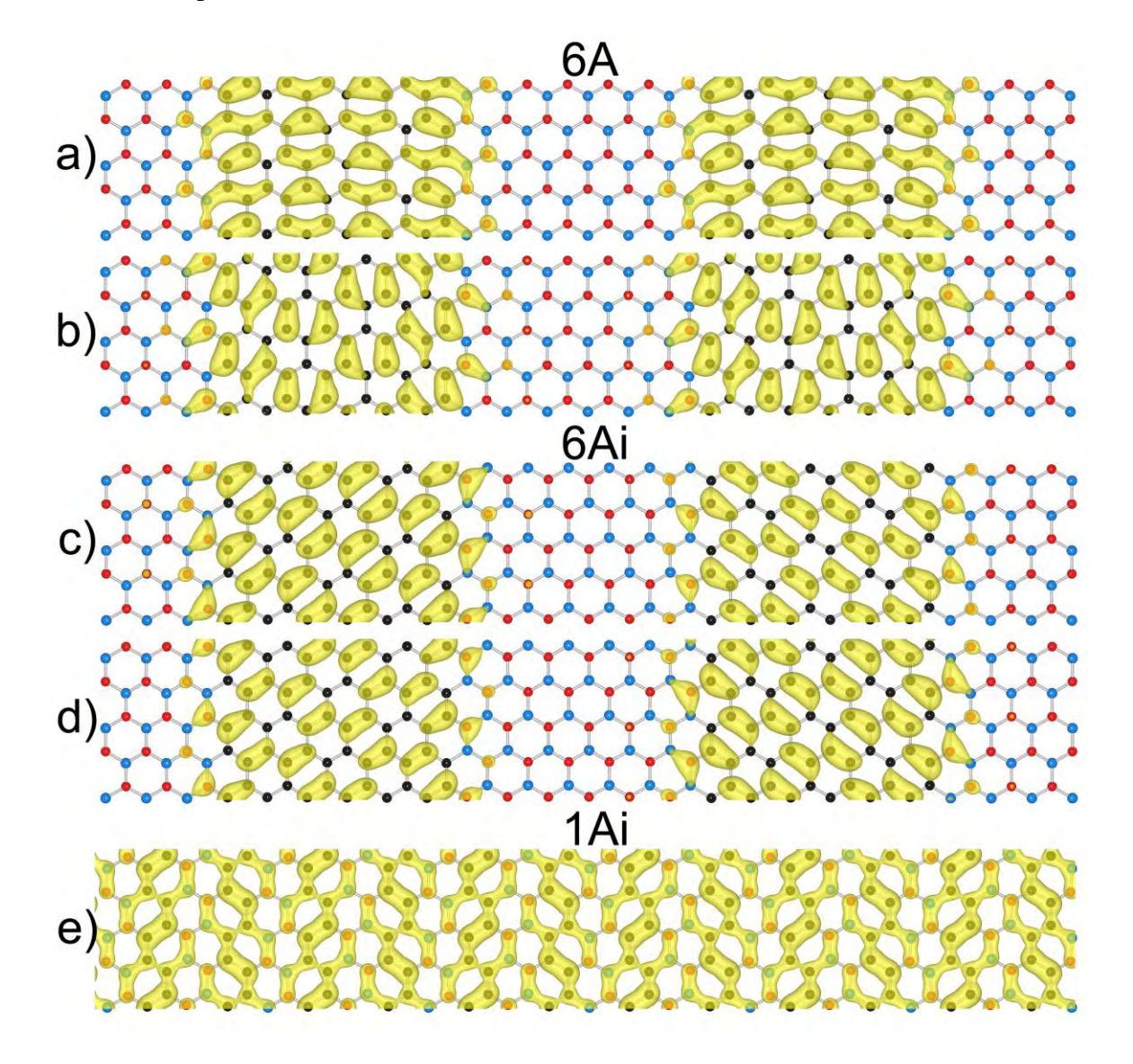


Table 1 The calculated structural parameters, total energy, and bandgap of 1-BN and graphene.

	1-BN	Graphene
Lattice constant (Å)	2.489	2.447
Bond length (Å)	1.437	1.413
Total energy (eV/pair)	-19.26	-20.19
Bandgap (eV)	4.61	-

References

- [1] K. S. Novoselov *et al.*, Science **306**, 666 (2004).
- [2] A. K. Geim, Science **324**, 1530 (2009).
- [3] A. H. Castro Neto et al., Rev. Mod. Phys. 81, 109 (2009).
- [4] A. K. Geim, and K. S. Novoselov, Nat. Mater. 6, 183 (2007).
- [5] K. S. Novoselov *et al.*, Nature **438**, 197 (2005).
- [6] S. Y. Zhou *et al.*, Nat. Phys. **2**, 595 (2006).
- [7] F. W. Averill, J. R. Morris, and V. R. Cooper, Phys. Rev. B **80**, 195411 (2009).
- [8] J. O. Sofo, A. S. Chaudhari, and G. D. Barber, Phys. Rev. B **75**, 153401 (2007).
- [9] X. Peng, and R. Ahuja, Nano Letters **8**, 4464 (2008).
- [10] B. Trauzettel *et al.*, Nat Phys **3**, 192 (2007).
- [11] M. Y. Han *et al.*, Physical Review Letters **98**, 206805 (2007).
- [12] L. Brey, and H. A. Fertig, Physical Review B **73**, 235411 (2006).
- [13] G. Giovannetti *et al.*, Physical Review B **76**, 073103 (2007).
- [14] C.-H. Park *et al.*, Nano Lett. **8**, 2920 (2008).
- [15] C.-H. Park et al., Phys. Rev. Lett. 101, 126804 (2008).
- [16] C.-H. Park et al., Phys. Rev. Lett. 103, 046808 (2009).
- [17] R. Pease, Acta Crystallogr. **5**, 356 (1952).
- [18] J. R. H. Wentorf, J. Chem. Phys. **34**, 809 (1961).
- [19] N. G. Chopra et al., Science **269**, 966 (1995).
- [20] X. Blase, Comput. Mater. Sci. 17, 107 (2000).
- [21] X. Blase et al., Appl. Phys. A 68, 293 (1999).
- [22] A. Rubio, J. L. Corkill, and M. L. Cohen, Phys. Rev. B 49, 5081 (1994).
- [23] X. Blase, and et al., Europhys. Lett. **28**, 335 (1994).
- [24] A. Y. Liu, R. M. Wentzcovitch, and M. L. Cohen, Phys. Rev. B **39**, 1760 (1989).
- [25] H. Şahin *et al.*, Phys. Rev. B **80**, 155453 (2009).
- [26] S. Azevedo, and R. d. Paiva, Europhys. Lett. **75**, 126 (2006).
- [27] H. Nozaki, and S. Itoh, J. Phys. Chem. Solids **57**, 41 (1996).
- [28] S. Azevedo, Eur. Phys. J. B 44, 203 (2005).
- [29] K. Yuge, Phys. Rev. B **79**, 144109 (2009).
- [30] M. Kawaguchi, T. Kawashima, and T. Nakajima, Chem. Mater. 8, 1197 (1996).
- [31] M. O. Watanabe *et al.*, Phys. Rev. Lett. **77**, 187 (1996).
- [32] Y. Chen et al., Phys. Rev. Lett. 83, 2406 (1999).
- [33] L. Ci et al., Nat. Mater. 9, 430 (2010).
- [34] E. Edlund, and M. N. Jacobi, Phys. Rev. Lett. **105**, 137203 (2010).
- [35] W. Kohn, and L. J. Sham, Phys. Rev. **140**, A1133 (1965).
- [36] D. M. Ceperley, and B. J. Alder, Phys. Rev. Lett. **45**, 566 (1980).
- [37] P. E. Blöchl, Phys. Rev. B **50**, 17953 (1994).
- [38] G. Kresse, and D. Joubert, Phys. Rev. B **59**, 1758 (1999).
- [39] G. Kresse, and J. Furthmüller, Comput. Mater. Sci. 6, 15 (1996).
- [40] G. Kresse, and J. Furthmüller, Phys. Rev. B **54**, 11169 (1996).
- [41] G. Kresse, and J. Hafner, J. Phys.: Condens. Matter **6**, 8245 (1994).
- [42] X. Blase et al., Phys. Rev. B **51**, 6868 (1995).
- [43] Y.-W. Son, M. L. Cohen, and S. G. Louie, Phys. Rev. Lett. 97, 216803 (2006).
- [44] We also performed calculations with the local spin density approximation to study spin ordered states at the domain edges. The ferromagnetic spin states at the edges are found to be unstable.
- [45] M. Fujita et al., J. Phys. Soc. Jpn. 65, 1920 (1996).
- [46] K. Nakada *et al.*, Phys. Rev. B **54**, 17954 (1996).

Print Page 1 of 2

From: prb@aps.org (prb@aps.org)

To: sirichok@gmail.com;

Date: Tue, May 17, 2011 2:54:49 AM

Cc:

Subject: Editorial Acknowledgment BE11710 Jungthawan

Re: BE11710

Electronic structures of graphene/boron nitride sheet superlattices by Sirichok Jungthawan, Sukit Limpijumnong, and Jer-Lai Kuo

Dear Dr. Jungthawan,

The editors acknowledge receipt of this manuscript on 11 May 2011 and are considering it as a Regular Article in Physical Review B. When sending correspondence regarding this manuscript please refer to the code number BE11710.

We understand your submission of this manuscript to certify the following:

- The paper represents original work of the listed authors.
- The manuscript as presented accurately reflects the scientific results.
- All of the authors made significant contributions to the concept, design, execution, or interpretation of the research study.
- All those who made significant contributions were offered the opportunity to be listed as authors.
- All of the listed authors are aware of and agree to the submission of this manuscript.
- The manuscript has not been published, and is not now and will not be under consideration by another journal while it is considered here.
- As part of the submission, the authors have provided any relevant information to the editors (e.g., information about recent relevant unpublished manuscripts by the authors).
- The authors accept the established procedures for selecting manuscripts for publication.

Please check the manuscript information and send us any corrections. The title, section, or PACS categories may have been changed from those provided by you on submission. To obtain current information regarding the status of your manuscript, you may consult the Author Status Inquiry System at http://authors.aps.org/STATUS/.

Yours sincerely,

Sarma Kancharla Assistant Editor Physical Review B Print Page 2 of 2

Email: prb@ridge.aps.org

Fax: 631-591-4141 http://prb.aps.org/

Physics - spotlighting exceptional research: http://physics.aps.org/

PRB Editors' Suggestions: http://prb.aps.org/#suggestions

Please verify the following information and notify the Editorial office of any corrections:

Code number: BE11710

Journal: PRB Regular Article

Received: 11 May 2011

Section: Surface physics, nanoscale physics, low-dimensional systems

PACS: 73.22.Pr

Complete PACS listings can be obtained via http://publish.aps.org/PACS/pacsgen.html

Address:

Dr. Sirichok Jungthawan School of Physics Suranaree University of Technology 111 University Avenue Nakhon Ratchasima 30000 THAILAND

Email: sirichok@gmail.com

Phone: Fax:

Title: Electronic structures of graphene/boron nitride sheet

superlattices

Collaboration:

3 Author(s):

Sirichok Jungthawan, Sukit Limpijumnong, Jer-Lai Kuo

FORMS AND MEMOS:

Please see the following:

http://forms.aps.org/author/rvwstndrds-au-prb.pdf
Physical Review B, review standards

Structural stability and electronic structure of monolayer BC₂N ordered structures

Sirichok Jungthawan^{1,2,3,*}, and Jer-Lai Kuo³

¹School of Physics, Institute of Science, Suranaree University of Technology and Synchrotron Light Research Institute, Nakhon Ratchasima 30000, Thailand ²Thailand Center of Excellence in Physics (ThEP), Commission on Higher Education, Bangkok 10400, Thailand

The structural stability of monolayer BC_2N is investigated by means of first-principles calculations. The formation energy monotonically decreases with increasing size of domains. The energetic favorable configurations have a strong preference of striped ordering (armchair or zigzag) with alternating domain of B-N and C-C ribbons formed by molecular chains. The systems provide information of electronics properties related of edge modification and inversion symmetry. The armchair and zigzag ordered structures have bandgaps which decrease as the number of chains increase. The inversion symmetry introduces zero bandgap in zigzag ordered structures but not in armchair ordered structures. The bandgap of armchair ordered structures exhibit triple periodicity feature and the structures without inversion symmetry always have nonzero bandgap. Detailed analysis on the electronic charge distributions show that the properties of the monolayer BC_2N compounds strongly depend on the size and the edge of domains.

E-mail address: sirichok@sut.ac.th

³Institute of Atomic and Molecular Sciences, Academia Sinica, Taipei 10617, Taiwan

Structural stability and electronic structure of monolayer BC₂N ordered structures

Sirichok Jungthawan (莊俊強)^{1,2,3,*} and Jer-Lai Kuo (郭哲來)³

¹School of Physics, Institute of Science, Suranaree University of Technology and

Synchrotron Light Research Institute, Nakhon Ratchasima 30000, Thailand

²Thailand Center of Excellence in Physics (ThEP Center), Commission on Higher

Education, Bangkok 10400, Thailand

³Institute of Atomic and Molecular Sciences, Academia Sinica, Taipei 10617, Taiwan

Abstract

The structural stability of monolayer BC2N is investigated by means of a first-

principles calculation. The direct enumeration method is used to generate a set of possible

atomic arrangements with up to 8 atoms per unit cell. The arrangements of the larger unit

cells are generalized from the information found in 8 atoms cell. The energetic favorable

configurations have a strong preference of stripe ordering, either armchair or zigzag, with

alternating domain of B-N and C-C molecular chains. The formation energy

monotonically decreases with increasing size of domains. With the same B-N fraction,

armchair ordered structures are more energetic favorable than zigzag ordered structures.

The armchair and zigzag ordered structures have bandgap which decreases as the number

of chains increase. The structures without inversion symmetry always have nonzero

bandgap. The properties of the monolayer BC₂N compounds strongly depend on the size

and the edge of domains.

E-mail address: sirichok@sut.ac.th

The Effects of Unit Cell Size on the Bandgap Range in the Direct Enumeration Study of Al_xGa_vIn_{1-x-v}P Alloys

Sirichok Jungthawan^{a,b,c}, Kwiseon Kim^d, and Sukit Limpijumnong^{a,b}

 ^aSchool of Physics, Institute of Science, Suranaree University of Technology and Synchrotron Light Research Institute, Nakhon Ratchasima 30000, Thailand
 ^bThailand Center of Excellence in Physics (ThEP Center), Commission on Higher Education, Bangkok 10400, Thailand

^cInstitute of Atomic and Molecular Sciences, Academia Sinica, Taipei 10617, Taiwan ^dNational Renewable Energy Laboratory, Golden, Colorado 80401, USA e-mail: sirichok@sut.ac.th

keywords: AlGaInP, direct enumeration, bandgap range, band interaction

Direct enumeration method is an unbiased approach for scanning alloy properties by computing all possible configurations. This method thoroughly covers all possible configurations within a given unit cell size; allowing one to extract informative trend of alloy properties with respect to ordering patterns. The larger cell means more number of possible configurations to be studied. However, in practice, the number of possible configurations increases rapidly with the size of the cell. Usually, a reasonable size that gives a sufficiently large number of configurations is chosen. In this work, the convergence of the bandgap range with respect to the unit cell size of AlGaInP alloy is studied up to 8 cation atoms per unit cell. It is found that the bandgap range already converges to within 0.1 eV at the unit cell size of 4 cation atoms. Interestingly, we also found that the lowest bandgap value of GaInP alloy is achieved already in a small cell (2 cations in the unit cell). The cause for this special small bandgap case is discussed.

References

- 1. S. Jungthawan, S. Limpijumnong, R. Collins, K. Kim, P. A. Graf, and J. A. Turner, *J. Appl. Phys.* **105**, 123531 (2009).
- 2. S. Jungthawan, K. Kim, and S. Limpijumnong, Comput. Mater. Sci., (accepted).

Name: Sirichok Jungthawan

Education:

2002-2008: Ph.D. in Physics, School of Physics, Suranaree University of Technology, Nakhon Ratchasima, Thailand

1997–2001: B.S. in Physics, Department of Physics, Srinakharinwirot University, Bangkok, Thailand

Professional Career:

2010: Postdoctoral fellow at Institute of Atomic and Molecular Sciences, Academia Sinica, Taipei 10617, Taiwan

2008-present: Lecturer in Physics, School of Physics, Suranaree University of Technology, Nakhon Ratchasima 30000, Thailand



A02209-04820

A02254-03840

Binary Semiconductors - A Theoretical Investigation

Rita JOHN¹; Pushpalatha S.¹; Sathya G. S.¹; Hannah Catherin D.²

1. Theoretical Physics, University of Madras, Tamil Nadu, India

2. P. G. Physics, Women's Christian College, Tamil Nadu, India

The binary semi-conductors and their alloys are gaining importance due to their dependable properties to suit most of the technical applications. An attempt is made to study the band structure of binary II-VI, AB: (A=Zn, Cd; B=S, Se, Te) and III-V, AB: (A=Al)Ga, In; B= P, As) semi-conductors and II-VI oxides, MgO, BeO, ZnO, and CdO using semi-relativistic Tight Binding Linear Muffin Tin Orbital (TBLMTO) method within local density approximation with von Barth Hedin exchange and correlation scheme. The present work investigates the band structure calculations for all the above mentioned compounds at ambient and high pressures. A systematic study of the equilibrium lattice parameters, nature of energy gap and metallization volume is reported. A high pressure study reveals band gap closure leading to metallization in all these compounds.

These binary compounds are investigated with respect to the parameters such as energy gap, bulk modulus, melting temperature, crystal potential and cell volume. The correlation between these parameters are brought out and compared with that of their ternary analogs I-III-VI2 chalcopyrites and II-IV-V₂ pnictides reported by us earlier. In all these comparative study, II-VI oxides show different trend when compared to other II-VI binary compounds which follow a particular trend. The reason for this varied trend of oxides is investigated and also linked to the quantum confinement observed in nano regime of these semiconductors. The trend of changes is exactly followed when these bulk semiconductors go nano. Quantum confinement, blue shift and crystal size and potential effects are also analyzed. The work is further extended to study the band structure of mixed binary compounds such as CdS_xSe_{1-x}

First-principles Study of Non-linear Dielectric Response for LaAlO₃/SrTiO₃ Superlattices

Shoji ISHIBASHI^{1;3}; Kiyoyuki TERAKURA^{1;2;3}

- 1. Research Institute for Computational Sciences, National Institute of Advanced Industrial Science and Technology, Tsukuba, Ibaraki, Japan
- 2. Research Center for Integrated Science, Japan Advanced Institute of Science and Technology, Nomi, Ishikawa, Japan
- 3. CREST, Japan Science and Technology Agency, Kawaguchi, Saitama, Japan

LaAlO₃(LAO)/SrTiO₃(STO) system has been attracting much attention because, for [001] stacking, the n-type interface (LaO-TiO₂) between two band insulators becomes metallic. It is thought that this phenomenon can be related to the polar-catastrophe problem. Recently, we have clarified how electronic and ionic mechanisms play to screen the diverging potential for LAO/STO thin films and found specific electronic states appear at the interface.

In the present study, we try to illustrate further anomalous behaviors of the interface between LAO and STO by calculating spatial distribution of dielectric response in LAO/STO superlattices for both [001] and [011] stacking. To do this, we have employed several special computational techniques. We have performed self-consistent electronic structure calculations under static electric field and, then, constructed maximally-localized one-dimensional Wannier functions to obtain local polarization distribution. All the calculations have been done with our in-house computational code QMAS (Quantum MAterials Simulator). In the obtained dielectric-constant profiles, non-linear behaviors, which are more pronounced at the interface region in the STO side, have been found.

A02309-04137

Direct Enumeration Studies of Band-Gap Properties of Al_xGa_yIn_{1-x-y}P Alloys

<u>Sirichok JUNGTHAWAN</u>^{1;2}; Kwiseon KIM³; Peter GRAF³; Sukit LIMPIJUMNONG^{1;2}

- 1. School of Physics, Suranaree University of Technology, Nakhon Ratchasima, Thailand
- 2. Synchrotron Light Research Institute, Nakhon Ratchasima, Thailand
- 3. National Renewable Energy Laboratory, Colorado, United States

AlGaInP alloys have potential applications in electronic devices and solar cells. The main advantage of this class of materials is that the band gap and lattice spacing can be simultaneously engineered. The properties of the band gap depend on both the alloy compositions and cation

arrangements. In this work, the band gap properties of Al_xGa_yIn_{1-x-y}P alloys have been studied by direct calculations of a large number of alloy configurations. A large number (~5000) of alloy configurations are generated using a direct enumeration approach. Then, the band gap properties of each configuration are calculated using the empirical pseudopotential method. We will present the ranges of possible band gaps and their types (direct or indirect) as functions of compositions. Our results show that the band gap of the AlGaInP alloy depends strongly on the cation arrangement in addition to the alloy composition. However, the band gap type is found to depend strongly on the composition and only weakly on the cation arrangements. A majority of alloy studied have band gaps smaller than those predicted by Vegard's law (downward bowing). The band gap reduction can be attributed to the ordering effects. We will also present some systematic trends of the band gaps with respect to the superlattice directions.

The work at NREL is supported by U.S. DOE under Contract No. DE-AC36-99G010337 and the Thailand Research Fund through the Royal Golden Jubilee Ph.D. Program (Grant No. PHD/0162/2547). The work in Thailand is supported by the Thailand Research Fund (Grant No. BRG5180001) and Commission on Higher Education (CHE-RES-RG "Theoretical Physics").

A02323-03979

Design and Fabrication of Quasi-multilayer Arrays for the Flat-band Pass Filters on UV-Vis Wavelength Region

Jong-Bin YEO¹; Hyun-Yong LEE²

1. Department of Functional Nano Fine Chemicals, Chonnam National University, Gwang-Ju, South Korea 2. Faculty of Applied Chemical Engineering, Chonnam National University, Gwang-Ju, South Korea

A simulator to optimize the structure conditions of onedimensional photonic quasi-crystals (1D PQCs) has been developed using a MATLAB program and ourself manufacturing calculation codes. The designed 1D PQCs structure were fabricated by sputtering, and their measured results were compared with calculated results.

Photonic crystals (PCs) require high refractive-index contrast periodic arrays to obtain omnidirectional photonic bandgaps (omni-PBGs) or electromagnetic stop bands. The PQCs are aperiodic arrays possessing long-range translation but short-range disorder, so that they exhibit high rotational symmetries and the omni-PBGs even at low index contrast array. Therefore, the PQCs are expected to be used for many applications in optoelectronics and optical communications.

In this work, We designed the 1D PQC arrays for application to the flat-band pass filters and fabricated on quartz substrate

by sputtering several dielectric targets such as SiO_2 , TiO_2 , ITO, Si and chalcogenides etc. A centre wavelength of filtering region is 460 nm. The optical transmittance of fabricated 1D PQCs was measured in a wavelength range of 250 \sim 800 nm using a UV-Visible spectrophotometer and compared with the calculated values. As a result, the fabricated PQCs exhibited optical characteristics in a good agreement with the calculation.

We believe that the PQC-based devices could be comprehensively applied to the new conceptional passive and active devices.

A02323-04003

Normalized Characteristics of the Photonic Bandgaps in Two-dimensional Photonic Quasicrystals with a Hexagonal Lattice by FDTD Simulation

Jong-Bin YEO1; Hyun-Yong LEE2

1. Department of Functional Nano Fine Chemicals, Chonnam National University, Gwang-Ju, South Korea 2. Faculty of Applied Chemical Engineering, Chonnam National University, Gwang-Ju, South Korea

Characteristics of the photonic bandgaps (PBGs) in twodimensional photonic quasicrystals (2D PQCs) with 8-fold have theoretically studied using a finite difference time domain (FDTD) simulation.

In this paper, we propose a concept of optical coverage ratio (OCR) as a new structural parameter to determine the PBGs for E-poloarized light. The OCR is an optically compensated filling factor. It is possible to normalize the PBGs of 2D PCs by introducing the OCR.

A02331-03990

3 Dimensional Printing of Pollution Absorbing Lamination Composites for Architectural Materials

Ginger DOSIER

Architecture, American University of Sharjah, Sharjah, United Arab Emirates

Air pollution continues to increase as construction and traffic contribute large amounts of hydrocarbons, carbon monoxide, and nitrogen oxides into the atmosphere. The objective of this research is to define the potential integration and implementation of a three-dimensional printed material surface that mitigates certain forms of air pollution.

Assimilating both the disciplines of architecture and material science, our collaborative research is currently developing architectural surfaces and units that absorb